Energy– and enstrophy–preserving discretisations of the incompressible Navier–Stokes equations

Matin Shams

St Hugh's College

University of Oxford

Submitted in partial completion of the

MSc in Mathematical Modelling and Scientific Computing

Trinity 2025

To the memory of Masoud Sharifi

Abstract

The typical energy estimate for the Navier–Stokes equations provides a bound for the gradient of the velocity; energy–stable numerical methods that maintain this estimate preserve this bound. However, the bound scales with the Reynolds number Re causing solutions to be numerically unstable (i.e., exhibit spurious oscillations) on under–resolved meshes. On the other hand, in the transient two–dimensional case the dissipation of enstrophy provides a bound for the gradient that is independent of Re.

We propose a finite–element integrator for the Navier–Stokes equations that preserves the evolution of both the energy and enstrophy, implying gradient bounds that are, in the 2D case, independent of Re. Our scheme is a mixed velocity–vorticity discretisation, using the idea of a discrete Stokes complex from finite element exterior calculus. While we introduce an auxiliary vorticity in the discretisation, the energy– and enstrophy–stability results both hold on the primal variable, the velocity; our scheme thus exhibits greater numerical stability at large Re than other methods in the literature. We conclude with a demonstration of numerical results.

Acknowledgements

What else is left to us, when the burden of the times grows too heavy, but to hide in the small act of shaping chaos into something that resembles order? And when the world you carry within yourself – the world that once rooted you most deeply – turns to ruins, what meaning can there be in symbols, equations, and proofs? Yet it is precisely here that I keep a vigil: mathematics, fragile though it is, a reminder to me that even amidst devastation, the mind can persist, create, and refuse to surrender.

To my advisors, Patrick Farrell and Boris Andrews, I owe more than guidance: I owe the gift of being accompanied in thought. They stood, each in their own way, as quiet architects of the path I now walk. Without their presence, the journey would have been lonelier, and the mathematics less alive.

To my family: your patience has been the truest form of strength, the silent rock that has carried me farther than these pages ever will.

Contents

List of Abbreviations

1D, 2D, 3D . . One–, two–, or three–dimensional; referring to the spatial dimension of the problem or domain under consideration.

AV . . . . . Auxiliary variable

BC . . . . . Boundary condition

BVP . . . . . Boundary–value problem

CG . . . . . Continuous Galerkin

DG . . . . . Discontinuous Galerkin

DoF . . . . . Degree of Freedom

FE . . . . . Finite element

FEEC . . . . . Finite element exterior calculus

GNI . . . . . Geometric numerical integration

IC . . . . . Initial condition

IPM . . . . . Interior penalty method

IVP . . . . . Initial–value problem

LHS . . . . . Left–hand side

MEEVC . . . Mass–, energy–, enstrophy–, vorticity–conserving

NS . . . . . Navier–Stokes

PDE . . . . . Partial differential equation

QoI . . . . . Quantity of interest

RHS . . . . . Right–hand side

SP . . . . . Structure–preserving/Structure preservation

Alles Gescheite ist schon gedacht worden.
Man muss nur versuchen, es noch einmal zu denken.

All intelligent thoughts have already been thought;
what is necessary is only to try to think them again.

— Johann Wolfgang von Goethe

1 Introduction

Contents

We begin with the incompressible Navier–Stokes equations

$$\dot{\mathbf{u}} = -\mathbf{u} \cdot \nabla \mathbf{u} - \nabla p + \frac{1}{\mathrm{Re}} \Delta \mathbf{u}, \tag{1.1a}$$

$$0 = \operatorname{div} \mathbf{u}, \tag{1.1b}$$

subject to an initial condition $\mathbf{u}(\mathbf{x}, 0) = \mathbf{u}_0$ and boundary conditions on a bounded Lipschitz domain $\Omega \subset \mathbb{R}^d$ with boundary $\partial\Omega$. Here, $\mathbf{u} : \mathbb{R}_+ \times \Omega \to \mathbb{R}^d$ denotes the time–dependent fluid velocity, $P : \mathbb{R}_+ \times \Omega \to \mathbb{R}$ the scalar pressure, and $\mathrm{Re} > 0$

the Reynolds number. The Laplacian Δ acts componentwise on $\mathbf{u}$, and $*$ indicates the partial derivative with respect to time t.

The existence of a smooth, globally defined solution to the three–dimensional incompressible Navier–Stokes (NS) equations remains an open problem. The strong form (1.1) tacitly demands high regularity i.e. $\mathbf{u}, p \in C^{2,1}$ in space–time[1]. Whether such regularity persists for all time in 3D is, as yet, unproven [Fef00]. In applications, one therefore computes numerically. Yet in the parameter ranges where numerical resolution is most demanding—typically large Re—fully resolving all scales in the solution space is infeasible[2]; most practical simulations are necessarily under–resolved. The usual palliatives—artificial viscosities, upwind penalties, spectral filters (see §1.1.4)—stabilise the numerics by altering the equation, damping the very features (fine–scale dynamics) one hopes to capture, and break reversibility in the Euler limit as $\mathrm{Re} \to \infty$.

This thesis, however, takes a different tack. The incompressible system carries rigid quadratic structure: kinetic energy in all dimensions, enstrophy in two, helicity in three. These invariants measure, respectively, the L^2–norm of the velocity $\mathbf{u}$, the $\mathbf{H}^1$–seminorm of the velocity (or, equivalently, the L^2–norm of its vorticity), and in three dimensions the cross–correlation $(\mathbf{u}, \operatorname{curl} \mathbf{u})$ known as helicity[3], which quantifies the linkage or knottedness of vortex lines. The question we pose is simple: *Does strict discrete adherence to the quadratic structures—energy and enstrophy—yield robust under–resolved simulations without artificial damping?* It does. We now turn to what is known: the results that inform this inquiry.

1.1 Related literature

We chart the ground briskly: the core results we build on, the techniques we modify, and the assumptions we decline.

[1] In parabolic Hölder notation, $C^{2,1}$ means two continuous spatial derivatives and one continuous time derivative, with the compatibility needed to interpret $(\mathbf{u}\cdot\nabla)\mathbf{u}$, $\Delta\mathbf{u}$, and ∇P pointwise.

[2] Low–Reynolds–number regimes are of equal physical interest—for example in microfluidics or porous–media flow—but the numerical difficulties motivating this work arise predominantly at high Re.

[3] Here $(\cdot,\cdot)$ denotes the inner product in $L^2(\Omega)$, i.e. $(\mathbf{a}, \mathbf{b}) = \int_\Omega \mathbf{a} \cdot \mathbf{b} \, \mathrm{d}\mathbf{x}$.

1.1.1 Energy preservation

Energy is the grammar of incompressible Navier–Stokes; the rest of the syntax hangs from it. The literature on the design of energy–stable integrators for the incompressible NS equations is vast. We can, however, trace its origins back to the late 1950s & 1960s: In 1959, Phillips [Phi59] observed that, when improperly handled, nonlinear advective terms could lead to the breakdown of solutions for numerical integrators; 7 years later Arakawa [Ara66] enforced conservation of certain quadratic norms on the solution; with early finite–difference instances in Harlow & Welch [HW65] and Arakawa, Mesinger & Lamb [MA76; AL77]. In 1970, Piacsek & Williams [PW70] then linked discrete energy balance to an L^2–skew (skew–adjoint[4]) convective operator.

1.1.2 Motivation: Stabilisation via enstrophy preservation

Although energy is the customary theme in discussing incompressible Navier–Stokes equations, the system exhibits further structure, especially in two dimensions. In particular, we highlight the enstrophy $\mathcal{E}(\mathbf{u}) := \frac{1}{2}\|\nabla\mathbf{u}\|^2$, where $\|\cdot\|$ denotes the $\mathbf{L}^2$ norm. Intuitively, enstrophy quantifies small–scale rotational content: a *vorticity energy* measuring the intensity of fine–scale turbulent motion. In parallel with the kinetic energy $\mathcal{K}(\mathbf{u}) := \frac{1}{2}\|\mathbf{u}\|^2$, which dissipates according to $\dot{\mathcal{K}} = -\frac{1}{\mathrm{Re}}\|\nabla\mathbf{u}\|^2$ (see §3.3.1), the enstrophy in 2D (under appropriate boundary conditions) dissipates as $\dot{\mathcal{E}} = -\frac{1}{\mathrm{Re}}\|\Delta\mathbf{u}\|^2$ (see §3.3.2), where Δ denotes the Laplacian.

In §3, we derive energy– and enstrophy–stable integrators for the incompressible Navier–Stokes equations, i.e. schemes that conserve energy in the inviscid limit (and dissipate for $\mathrm{Re} < \infty$) and preserve the evolution—or dissipation in 2D—of enstrophy. By contrast, typical $\mathbf{H}^1$–conforming schemes that are only energy–stable struggle on under–resolved meshes—formally, when $h^2\mathrm{Re} \gg 1$ for a given mesh size h. The tell–tale symptom is the appearance of large, spurious velocity oscillations.

While many explanations can be offered for this phenomenon (see §1.1.4), we trace the effect to the absence of a meaningful $\mathbf{H}^1$ a priori estimate holding on the discrete solution: in finite dimensions, norm equivalence already converts an $\mathbf{L}^2$ bound into an $\mathbf{H}^1$ bound up to a mesh–dependent constant. Yet, the classical energy estimate

[4] An operator $\mathcal{C}$ is *skew–adjoint* if $(\mathcal{C}\mathbf{u}, \mathbf{v}) = -(\mathbf{u}, \mathcal{C}\mathbf{v})$ for all $\mathbf{u}, \mathbf{v}$. For the convective operator $\mathcal{C}(\mathbf{u})\mathbf{v} = (\mathbf{u}\cdot\nabla)\mathbf{v}$, this holds when $\mathrm{div}\mathbf{u} = 0$, so that $(\mathcal{C}(\mathbf{u})\mathbf{u}, \mathbf{u}) = 0$, expressing kinetic–energy conservation.

(1.2) scales with Re and, as $\mathrm{Re} \to \infty$, fails to control $\|\nabla \mathbf{u}\|$. In the continuous setting, the standard estimates (cf. §3.3.1) read as follows

$$\sup_{t \geq 0} \|\mathbf{u}\|^2 \;\leq\; \|\mathbf{u}(0)\|^2, \qquad \int_0^\infty \|\nabla \mathbf{u}\|^2 \;\leq\; \frac{\mathrm{Re}}{2} \|\mathbf{u}(0)\|^2. \tag{1.2}$$

Therefore, when $h^2\mathrm{Re} \gg 1$, the $\mathbf{H}^1$ bound no longer constrains the discrete solution beyond what the $\mathbf{L}^2$ bound already provides and exerts no additional regularising force on $\mathbf{u}$. $\mathbf{H}^1$–conforming discretisations that are solely energy–stable therefore lack any barrier to the growth of fine–scale oscillations on coarse meshes and at high Reynolds numbers Re. In the Euler case, $\mathrm{Re} = \infty$, the claim is immediate; no $\mathbf{H}^1$ bound is available at all.

Figure 1.1 illustrates this phenomenon for an energy–stable $\mathbf{H}^1$–conforming scheme applied to the advection of a two dimensional vortex. At moderate Reynolds number $\mathrm{Re} = 2^{12}$, the vortex advects smoothly around the perimeter of the domain $\Omega = (0,1)^2$ as expected. However, as Re increases, the loss of a meaningful $\mathbf{H}^1$ bound becomes apparent: spurious oscillations emerge and distort the solution, despite energy stability being maintained. The scheme thus fails to replicate the expected dynamics—in this setup[5], a vortex orbiting clockwise around the perimeter of the domain Ω.

One therefore requires an Re–robust $\mathbf{H}^1$ bound, i.e. independent of Re. In two dimensions, and again under suitable boundary conditions (i.e. Assumption 2.1), such a bound arises from enstrophy dissipation (see §3.3.2). In the continuous case, we have

$$\sup_{t \geq 0} \|\nabla \mathbf{u}\|^2 \;\leq\; \|\nabla \mathbf{u}(0)\|^2, \quad \int_0^\infty \|\Delta \mathbf{u}\|^2 \;\leq\; \frac{\mathrm{Re}}{2} \|\nabla \mathbf{u}(0)\|^2. \tag{1.3}$$

In particular, this yields an Re–robust $\mathbf{H}^1$ bound, together with an $\mathbf{H}^2$ bound that scales with the Reynolds number Re. In contrast to the energy–based $\mathbf{H}^1$ estimate, the enstrophy–driven one remains meaningful as $\mathrm{Re} \to \infty$, even in the inviscid Euler limit $\mathrm{Re} = \infty$. This motivates the use and construction of enstrophy–stable schemes, as they are expected to offer improved stability over solely energy–stable ones on under–resolved meshes in two dimensions. We demonstrate this improved stability in §5.

[5] The vortex configuration follows the setup described in §5.2.

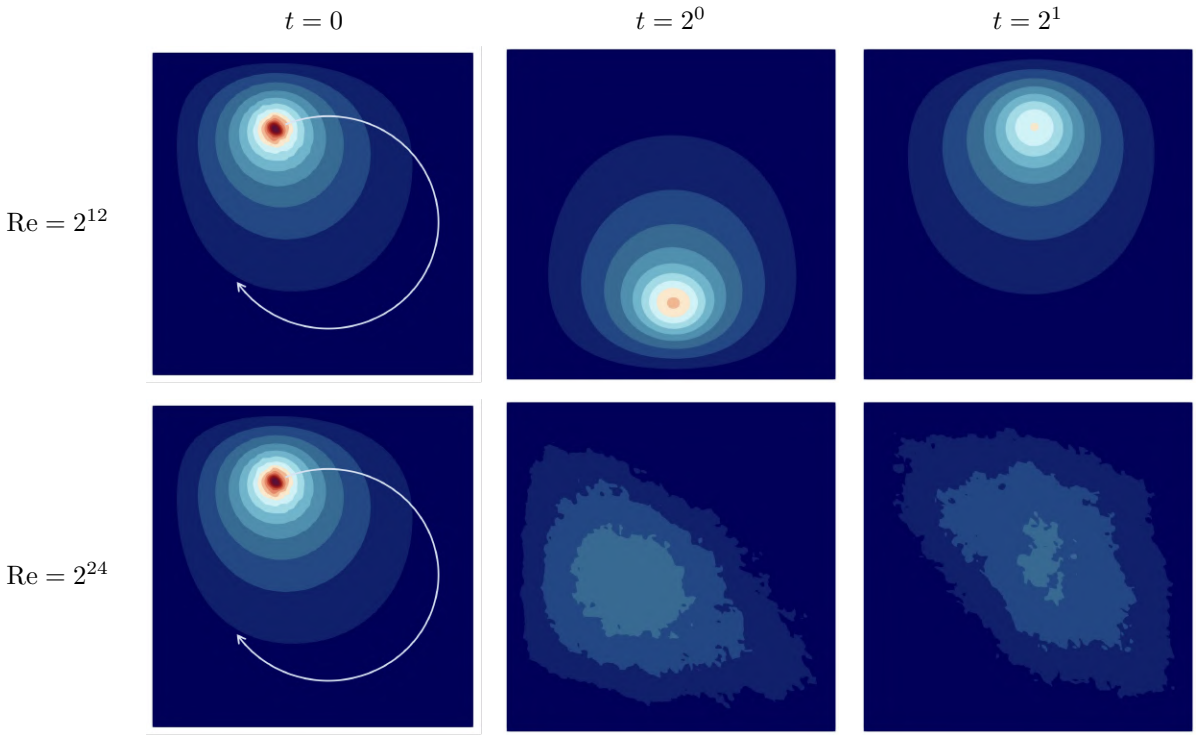

Figure 1.1: Snapshots of an energy–stable $\mathbf{H}^1$–conforming scheme for $\mathrm{Re} = 2^{12}$ and $\mathrm{Re} = 2^{24}$ at times $t \in \{0, 2, 2\}$.

1.1.3 3D Enstrophy

In 2D, we saw that enstrophy conservation supplies a meaningful $\mathbf{H}^1$ bound independent of Re—providing control of $\|\nabla \mathbf{u}\|$ even as $\mathrm{Re} \to \infty$. The three–dimensional setting, however, is fundamentally different: Euler conserves energy and helicity $\mathcal{H} := \frac{1}{2}(\mathbf{u}, \operatorname{curl} \mathbf{u})$, the latter being a topological measure of knottedness or linkage of vortex lines. In three dimensions, Robinson [Rob20] argues that energy conservation alone provides a handle on the global existence of weak solutions, whereas enstrophy is linked to the existence of strong (smooth) solutions. Enstrophy can be viewed as an indicator of solution regularity: as long as $\|\operatorname{curl} \mathbf{u}\|^2$ remains bounded, vorticity does not blow up, and no singularity can form. Conversely, any finite–time blowup (if it occurs) would necessarily involve enstrophy diverging to infinity. This is why enstrophy is often highlighted in regularity criteria—for example, one equivalent way to state the Clay Millennium Problem is: prove that for smooth initial data, $\mathcal{E}(t)$ cannot blow up in finite time.

Complementing the analytical picture, recent optimization–based computations by Kang et al. [KYP20] have probed worst–case enstrophy growth permitted by

the 3D Navier–Stokes equations. Kang et al. [KYP20] cast a family of PDE–constrained problems: among all initial data with prescribed enstrophy $\mathcal{E}_0$, find those that maximize enstrophy at time T. Large–scale adjoint methods reveal that the maximal amplification is finite at all times and there is no evidence of singularity formation. In 3D, one cannot hope to conserve enstrophy, but one may seek a discretisation that at least does not blow up enstrophy. In practice, no numerical scheme can prevent a real physical singularity if one were to occur—but if the scheme does tend to keep enstrophy bounded where the real physics would, it can be considered a stable and physically meaningful method. This is demonstrated with an exploratory 3D test in §5.3.

1.1.4 Stabilisation on under–resolved meshes

Conventional stabilisation techniques have failed to consider enstrophy stability, with the predominant strategy for $\mathbf{H}^1$–conforming schemes being the implementation of an artificial viscosity. Spectral vanishing viscosity (SVV) methods, originally introduced by Maday & Tadmor [MT89] in 1989, selectively apply dissipation to high–order modes; mitigating spurious oscillations that originate from energy accumulation at smaller spatial scales. Tadmor [Tad90; Tad93] established that, with carefully tuned parameters, SVV methods converge to entropy solutions; yet this targeted dissipation sacrifices the fidelity of the highest spectral modes, diminishing the effective resolution of the scheme.

The continuous interior penalty (CIP) and gradient jump penalisation (GJP) methods, first introduced by Douglas Jr. & Dupont [DD76], mitigate fine–scale oscillations by penalising jumps in the solution gradient over mesh interfaces. These methods have been rigorously analysed for advection–diffusion systems, including the incompressible Navier–Stokes equations at high Reynolds numbers, by Burman, Hansbo, & Fernández [BH04; BFH06; BF07]. At moderate polynomial orders (e.g. $p \approx 3$), where only a few high–order modes are present, CIP/GJP methods have been shown to outperform SVV schemes [Mou+22]. However, we note that the inclusion of artificial dissipation renders these methods irreversible in the Euler limit $\mathrm{Re} = \infty$.

In contrast, DG methods [CKS00] incorporate built–in upwind stabilisation, which naturally targets high–frequency components and favours finer spatial scales, as discussed by Moura et al. [MSP15; Mou+17]. Although DG methods exhibit stability properties akin to those of CIP and GJP approaches, they are often accompanied by a nontrivial increase in computational overhead, stemming from the higher number of degrees of freedom required for the same approximation order on an identical mesh.

1.1.5 Geometric numerical integration (GNI)

Physical quantities are intrinsically linked to geometry and orientation. If we properly capture these concepts in our mathematical descriptions of reality, certain structures naturally and consistently arise within physical equations. Differential geometry provides us with the mathematical description we need to identify these structures, as discussed by Tonti [Ton71; Ton88] who classifies physical problems on the basis of geometry. Fundamental to this classification is the distinction between metric–dependent and –independent relationships; the former being constitutive laws, and the latter being differential relations prescribed by the laws of physics. Tonti defines this structure in terms of two distinct classes: *source* variables and *configuration* variables, representing two distinct orientations of the same geometry. This same classification is also made by Frankel [Fra11], who refers to real and pseudo-forms, and by Bossavit [Bos98], referring to *straight* and *twisted* forms. Structure–preserving (SP) methods aim to retain this at the discrete or computational level [Ger12]. The close relationship between differential geometry and algebraic topology provides a crucial tool for translating these structures into numerical discretisation [Ton71; BH06; KPG11]. These analogs ensure that the metric–free relationships are preserved in the discrete setting, a fundamental component of SP frameworks.

Finite element exterior calculus (FEEC) [Hip01; AFW06; AFW09; Arn18; Hu25] plays the same role; it provides a systematic framework for constructing finite element spaces that respect geometric and topological structure of the underlying differential equations. In this setting, by choosing commuting subcomplexes of the de Rham/Stokes complex, the metric–free identities are carried onto the mesh: $\mathrm{curl} \circ \mathrm{grad} = 0$ and $\mathrm{div} \circ \mathrm{curl} = 0$ hold, and the projections commute with the differential operators. The orientation split persists: configuration (inner–oriented) variables live on the primal complex, source (outer–oriented) variables on the dual. Thus, the discrete scheme preserves the topological laws exactly, leaving only metric terms to approximate. In time, SP integrators propagate the same geometry [Ske95; BP03; HLW06; CMO11; BC17; IQ18].

We adopt the auxiliary–variable (AV) framework of Andrews & Farrell [AF25], which provides a general strategy for enforcing multiple conservation laws and dissipation inequalities in numerical time integration. In this approach, each conserved or dissipated quantity is associated with an auxiliary variable representing the projection of its test function onto a discrete test set; the governing equations are then modified to evolve these new variables alongside the primary unknowns. We incorporate this AV framework within a FEEC–based spatial discretisation (as

developed in §3), thereby combining its algebraic conservation mechanism with the geometric exactness of FEEC to obtain a structure–preserving velocity–vorticity formulation of the incompressible Navier–Stokes equations. Gauss–Legendre time stepping is used so that the quadratic invariants—energy, and in two dimensions, enstrophy—are preserved.

1.1.6 Novel aspects

Our scheme is a mixed velocity–vorticity discretisation relying on the existence of a discrete Stokes complex:

$$\begin{array}{ccccccc} H^1 & \xrightarrow{\text{grad}} & \mathbf{H}(\operatorname{grad}\operatorname{curl}) & \xrightarrow{\text{curl}} & \mathbf{H}^1 & \xrightarrow{\text{div}} & L^2 \\ \downarrow & & \downarrow & & \downarrow & & \downarrow \\ \overline{\mathbb{Q}} & \xrightarrow{\text{grad}} & \overline{\mathbb{V}} & \xrightarrow{\text{curl}} & \mathbb{V} & \xrightarrow{\text{div}} & \mathbb{Q} \end{array} \tag{1.4}$$

Our proposed semi–discretisation is as follows: find $(\mathbf{u}, p, \boldsymbol{\omega}, \theta) \in \mathbb{V} \times \mathbb{Q} \times \overline{\mathbb{V}} \times \overline{\mathbb{Q}}$ such that[6]

$$\int_\Omega \dot{\mathbf{u}} \cdot \mathbf{v} \,\mathrm{d}\mathbf{x} = \int_\Omega (\mathbf{u} \times \boldsymbol{\omega}) \cdot \mathbf{v} + p\,(\operatorname{div}\mathbf{v}) \,\mathrm{d}\mathbf{x} - \frac{1}{\mathrm{Re}} \int_\Omega \operatorname{curl}\boldsymbol{\omega} \cdot \mathbf{v} \,\mathrm{d}\mathbf{x}, \tag{1.5a}$$

$$0 = \int_\Omega (\operatorname{div}\mathbf{u})\, q \,\mathrm{d}\mathbf{x}, \tag{1.5b}$$

$$\int_\Omega \operatorname{curl}\boldsymbol{\omega} \cdot \operatorname{curl}\boldsymbol{\chi} \,\mathrm{d}\mathbf{x} = \int_\Omega \operatorname{curl}\mathbf{u} \cdot \operatorname{curl}^2\boldsymbol{\chi} \;-\; \nabla\theta \cdot \boldsymbol{\chi} \,\mathrm{d}\mathbf{x}, \tag{1.5c}$$

$$0 = \int_\Omega \boldsymbol{\omega} \cdot \nabla\eta \,\mathrm{d}\mathbf{x}, \tag{1.5d}$$

for all $(\mathbf{v}, q, \boldsymbol{\chi}, \eta) \in \mathbb{V} \times \mathbb{Q} \times \overline{\mathbb{V}} \times \overline{\mathbb{Q}}$. The auxiliary variable $\boldsymbol{\omega}$ is a discretely divergence–free approximation to the vorticity $\operatorname{curl}\mathbf{u}$. This preserves discrete forms of energy dissipation and the evolution of enstrophy,

$$\partial_t \left[\frac{1}{2}\int \|\mathbf{u}\|^2\right] = -\frac{1}{\mathrm{Re}}\int \|\operatorname{curl}\mathbf{u}\|^2, \tag{1.6a}$$

$$\partial_t \left[\frac{1}{2}\int \|\operatorname{curl}\mathbf{u}\|^2\right] = -\int \mathbf{u}\cdot(\boldsymbol{\omega}\cdot\nabla\boldsymbol{\omega}) \;-\; \frac{1}{\mathrm{Re}}\int \|\operatorname{curl}\boldsymbol{\omega}\|^2; \tag{1.6b}$$

as quadratic structures, these are preserved to the fully discrete level when using any Gauss–Legendre timestepping scheme. Notably, while we introduce an auxiliary vorticity $\boldsymbol{\omega}$, the energy and enstrophy stability results (1.6) both hold on the primal variable $\mathbf{u}$. In 2D, the equivalent scheme makes use of a discrete 2D Stokes complex.

[6] $\Omega \subset \mathbb{R}^d$ is a bounded, contractible domain with Lipschitz $\delta\Omega$, and Lebesgue measure $\mathrm{d}\mathbf{x}$.

In this case, the enstrophy evolution (1.6b) becomes a dissipation law, providing a Re–robust H^1 bound for $\mathbf{u}$, consequently offering greater numerical stability even in the ideal limit $\mathrm{Re} = \infty$. In contrast to existing stabilisation techniques (see §1.1.4), this necessitates the introduction of no artificial viscosities or penalty terms.

1.2 Code availability

The numerical code used to generate the results in this work was implemented in the `Firedrake` finite element framework [Ham+23], employing `UFL` [Aln+14] for the specification of variational forms and Gauss methods via `Irksome` [FKM21]. The codebase was written entirely in Python, and the resulting datasets were post–processed and visualized using `ParaView` [AGL05]. Code for reproducing results of this work is available at the GitHub repository: [Sha25].

1.3 AI Input

Generative AI tools were used solely to assist with LaTeX formatting and syntax, as well as to support debugging and clarify the functioning of certain code components. They were also used to paraphrase my own writing and correct grammar to bring the prose to an academic standard. This language support helps level the playing field for students whose first language is not English, while the intellectual content, arguments, and results remain entirely my own. Importantly, prose is not mere ornament: clarity and style shape how arguments are understood. To borrow a literary analogy, as James Joyce's work illustrates, form can carry meaning; improving form can therefore improve access to the underlying ideas. I affirm that no AI assistance was used for generating original research content, mathematical theorem/arguments, or citations, in accordance with the University of Oxford's AI usage policies [Oxf25].

1.4 Overview

This thesis has a simple rhythm: ideas first, machinery second, evidence last. Chapter 2 sets the stage. It weaves the strands of the literature that this work relies on and fixes the notation and preliminaries we use throughout. The aim is not encyclopaedia but orientation; enough background to read what follows.

Chapter 3 builds the discretisation. Starting from a velocity–pressure standard formulation, we construct a scheme that preserves the canonical 2D Euler invariants (energy and enstrophy). We also prove the core structure–preserving properties that motivate the method. Chapter 4 moves from theory to practice. In 3D, conforming implementations of the required spaces—notably $\mathbf{H}(\mathrm{curl}^2)$ and $\mathbf{H}(\mathrm{grad}\,\mathrm{curl})$—are not generally available in finite–element software (i.e. `Firedrake` [Ham+23]). We show how to overcome this. We also develop a non–conforming variant via an interior–penalty construction that will be used later in the experiments.

Chapter 5 is the proving ground. We run deliberately under–resolved tests (formally, $\mathrm{Re} = \infty$) to stress the schemes: a shear–layer problem and a 2D vortex test, where we measure the stabilising effect against traditional methods; and an exploratory 3D case, asking a pointed question–when enstrophy is no longer a conservation law, does tracking its evolution still yield qualitative gains? We let the computations answer. Chapter 6 closes the loop with a discussion and a short outlook. We summarise what stability buys us in practice, what it does not, and which extensions look most promising next.

A good notation has a subtlety and suggestiveness which at times make it seem almost like a live teacher.

— Bertrand Russell

2

Notation & preliminaries

This chapter fixes the language and standing hypotheses used throughout. We recall the minimal functional–analytic framework and fix conventions that underpin our discretisations. Proofs and broader generality in the differential–forms setting—finite element exterior calculus—are deferred to [Hip01; AFW06; AFW09; Arn18; Hu25].

Domain topology. All analysis henceforth will be conducted under the following assumptions on the domain Ω.

Assumption 2.1 (Domain, topology, and boundary)**.** *Throughout, if not otherwise specified, we work on a domain $\Omega \subset \mathbb{R}^d$, $d \in \{2, 3\}$, with the following properties:*

i) Regularity. Ω is bounded and Lipschitz[a]*. Whenever elliptic regularity e.g., in Lemma 2.2 is invoked, we additionally assume $\partial\Omega \in C^{2,1}$* [b]*.*

ii) Topology. Ω is contractible and topologically trivial (equivalent homotopy to a one–point space).

iii) Boundary conditions. Navier–slip BCs.

[a] Lipschitz boundary ensures the existence of a well–defined trace operator, allowing scalar–valued functions in $H^1(\Omega)$ to have traces in $H^{1/2}(\delta\Omega)$, which is necessary for imposing Dirichlet BCs in the model problem.

[b] i.e. locally $\partial\Omega$ is the graph of a function whose second derivatives are Lipschitz continuous.

Continuous problem formulation. The evolution of Newtonian viscous incompressible flows is governed by the Navier–Stokes equations (1.1). The NS equations differ from the closely related Euler equations through the presence of the viscous term $\frac{1}{\mathrm{Re}}\Delta\mathbf{u}$, which yields a quasilinear parabolic velocity equation and fixes the pressure via an elliptic constraint enforcing incompressibility. This diffusive term improves analytic properties–e.g., local well-posedness in 3D for smooth data and global well–posedness in 2D–at the expense of the geometric (Hamiltonian/Lie–Poisson) structure and its invariants (energy; along with enstrophy in 2D, and helicity in 3D) present in the Euler system [Fef00; AK08].

Options for the convective term. The nonlinear advective term $\mathbf{u}\cdot\nabla\mathbf{u}$ (see Equation 1.1) admits several equivalent formulations, each revealing different analytical or geometric properties of the equations. There are, in fact, many ways to express the convective term $\mathbf{u}\cdot\nabla\mathbf{u}$; we recall here the most common ones used in structure–preserving and energy–stable discretisations.

These equivalent expressions follow from the following tensor identity, which relates the advective and divergence forms of the nonlinear term.

$$\nabla\cdot(\mathbf{u}\otimes\mathbf{u}) = (\mathbf{u}\cdot\nabla)\mathbf{u} + (\nabla\cdot\mathbf{u})\mathbf{u}. \tag{2.1}$$

The first alternative formulation we consider, the skew–symmetric form, is obtained as a linear combination of the convective and divergence forms, so called because, once cast into a weak formulation, it defines a skew–symmetric form regardless of whether the divergence–free condition (1.1b) is enforced,

$$\dot{\mathbf{u}} = -\frac{1}{2}\mathbf{u}\cdot\nabla\mathbf{u} + -\frac{1}{2}\nabla\cdot(\mathbf{u}\otimes\mathbf{u}) - \nabla p + \frac{1}{\mathrm{Re}}\Delta\mathbf{u}, \tag{2.2a}$$

$$0 = \operatorname{div}\mathbf{u}. \tag{2.2b}$$

Another alternative, the rotational or Lamb form, using $(\mathbf{u}\cdot\nabla)\mathbf{u} = \nabla(\frac{1}{2}|\mathbf{u}|^2) - \mathbf{u}\times(\operatorname{curl}\mathbf{u})$, is

$$\dot{\mathbf{u}} = \mathbf{u}\times\operatorname{curl}\mathbf{u} - \nabla P + \frac{1}{\mathrm{Re}}\Delta\mathbf{u} \tag{2.3a}$$

$$0 = \operatorname{div}\mathbf{u}. \tag{2.3b}$$

In (2.3), $\times$ denotes the cross product, and $P = p + \frac{1}{2}|\mathbf{u}|^2$ is the total/Bernoulli pressure[1]. With some re–arranging, one may confirm that both (2.2) and (2.3) are equivalent to (1.1). However, only in the skew–symmetric form[2] (2.2) and the rotational form (2.3) the convective term vanishes, when the momentum equation is

[1] With a slight abuse of notation, we use p to denote the total pressure in the next chapters.

[2] Since $(\mathbf{u}, (\mathbf{u}\cdot\nabla)\mathbf{u} + \nabla\cdot(\mathbf{u}\otimes\mathbf{u})) = 0$; the convective term vanishes.

tested against $\mathbf{u}$. Therefore (unless $\operatorname{div}\mathbf{u} = 0$ holds *exactly*, in the discrete setting) either of these forms have to be used if we wish to have an energy dissipative scheme (and conserving in the inviscid limit $\mathrm{Re} = \infty$). Also, Piacsek & Williams [PW70] and Arakawa [Ara66] show that to avoid nonlinear instability, the discrete convective operator must be skew–adjoint.

Complexes and operators. Fluid models carry two layers of structure. Some relations are *topological*—they hold before any metric is chosen. Others are *metric*—they quantify energies and dissipation once an inner product is fixed. A structure–preserving discretisation must respect the topology *exactly* and the metric *compatibly*. We encode the topological layer through a Hilbert complex[3]

$$\cdots \longrightarrow X_{r-1} \xrightarrow{d_{r-1}} X_r \xrightarrow{d_r} X_{r+1} \xrightarrow{d_{r+1}} X_{r+2} \longrightarrow \cdots \tag{2.4}$$

where X_r is a Hilbert space and $d_r : X_r \to X_{r+1}$ is a bounded linear operator with $d_{r+1} \circ d_r = 0$. We write $\mathcal{N}d_r \subseteq X^r$ for its nullspace and $\mathcal{R}d_r \subseteq X^{r+1}$ for its range; the complex is exact at level–r when

$$\mathcal{N}(d_r) = \mathcal{R}(d_{r-1}). \tag{2.5}$$

Notational conventions. Let $\|\cdot\|$ and $(\cdot,\cdot)$ denote the L^2 norm and the L^2 inner product, respectively. With a slight abuse of notation, we use L^2 to denote both the scalar and vector L^2 spaces.

de Rham complexes. The operators in (2.3) are not ad hoc; they fit together in a rigid algebra,

$$\operatorname{curl} \circ \operatorname{grad} = 0, \qquad \operatorname{div} \circ \operatorname{curl} = 0. \tag{2.6}$$

We therefore work in the Hilbert spaces

$$H^1 := \left\{ v \in L^2(\Omega) : \nabla v \in L^2(\Omega) \right\}, \tag{2.7a}$$

$$\mathbf{H}(\operatorname{curl}) := \left\{ \mathbf{v} \in L^2(\Omega) : \operatorname{curl}\mathbf{v} \in L^2(\Omega) \right\}, \tag{2.7b}$$

$$\mathbf{H}(\operatorname{div}) := \left\{ \mathbf{v} \in L^2(\Omega) : \operatorname{div}\mathbf{v} \in L^2(\Omega) \right\}, \tag{2.7c}$$

arranged into the de Rham complex

$$H^1 \xrightarrow{\operatorname{grad}} \mathbf{H}(\operatorname{curl}) \xrightarrow{\operatorname{curl}} \mathbf{H}(\operatorname{div}) \xrightarrow{\operatorname{div}} L^2. \tag{2.8a}$$

[3] Geometrically, potentials live on nodes, circulations along edges, fluxes across faces, and densities in volumes; the incidence of these carriers is the discrete shadow of the differential operators; gradients accumulate along edges, curls around faces, and divergences across volumes.

The discrete counterpart of the de Rham complex (2.8a) is obtained by choosing finite–element spaces that preserve the exactness of the continuous sequence. In three dimensions, this corresponds to assigning degrees of freedom to geometric entities of the mesh—vertices, edges, faces, and cells—so that each operator acts locally between adjacent dimensions. This construction ensures that (2.6) hold exactly at the discrete level.

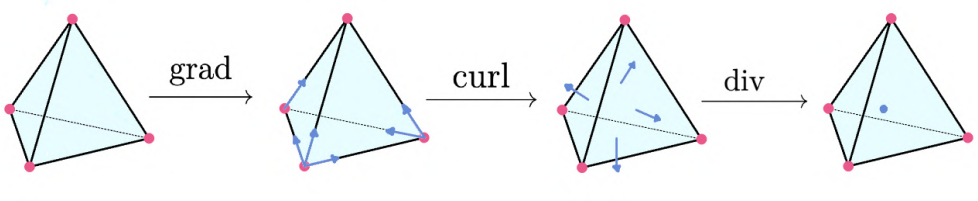

Figure 2.1: Discrete representation of the de Rham complex (2.8a). Degrees of freedom correspond to geometric entities of the mesh: scalar potentials at vertices, edge circulations for $\mathbf{H}(\mathrm{curl})$ fields, face fluxes for $\mathbf{H}(\mathrm{div})$ fields, and cell integrals for L^2 quantities.

In 2D, curl is a mapping from scalars to vectors, defined as $\operatorname{curl} v := (\partial_{x_2} v, -\partial_{x_1} v)$. Hence, (2.8a) reduces to

$$H^1 \xrightarrow{\ \mathrm{curl}\ } \mathbf{H}(\mathrm{div}) \xrightarrow{\ \mathrm{div}\ } L^2. \tag{2.8b}$$

Stokes complexes. Equation 2.8a records that each operator annihilates the last, yet the existence of a well–defined enstrophy requires higher regularity; we need $\mathbf{u}$ to lie in $\mathbf{H}^1$. We therefore make use of a Stokes complex, i.e. a de Rham complex with enhanced smoothness. While different forms for the Stokes complex exist we use

$$H^1 \xrightarrow{\ \mathrm{grad}\ } \mathbf{H}(\operatorname{grad}\operatorname{curl}) \xrightarrow{\ \mathrm{curl}\ } \mathbf{H}^1 \xrightarrow{\ \mathrm{div}\ } L^2, \tag{2.9}$$

where

$$\mathbf{H}(\operatorname{grad}\operatorname{curl}) := \left\{ \mathbf{v} \in \mathbf{H}(\mathrm{curl}) : \operatorname{curl} \mathbf{v} \in \mathbf{H}^1 \right\}. \tag{2.10}$$

In 2D, (2.9) reduces to

$$H^2 \xrightarrow{\ \mathrm{curl}\ } \mathbf{H}^1 \xrightarrow{\ \mathrm{div}\ } L^2. \tag{2.11}$$

In §3, we choose finite–element subcomplexes with commuting L^2 projections so that the Stokes algebra and the required regularity persist at the discrete level.

Boundary conditions. We impose boundary conditions that are intrinsic to the function spaces we inhabit: not an afterthought, but the boundary traces that let

the de Rham/Stokes complexes close and that eliminate boundary terms in the integrations by parts used later. In 3D, we work with the Navier–slip BCs,

$$\operatorname{curl}\mathbf{u}\times\mathbf{n}=0,\quad\text{and}\quad\mathbf{u}\cdot\mathbf{n}=0. \tag{2.12}$$

Here, $\mathbf{n}$ denotes the outward–pointing unit normal vector on $\partial\Omega$, and $\mathbf{t}$ denotes any unit tangential vector. Equation 2.12 is simply the no–tangential–stress BC

$$\mathbf{t}\cdot\Big(\nabla\mathbf{u}+(\nabla\mathbf{u})^{\top}\Big)\mathbf{n}=0\quad\text{for all tangents }\mathbf{t}, \tag{2.13}$$

written in the language of the complex: under $\mathbf{u}\cdot\mathbf{n}=0$ the two BCs satisfy $\mathbf{t}\cdot(\nabla\mathbf{u}+\nabla\mathbf{u}^{\top})\mathbf{n}=\mathbf{t}\cdot(\operatorname{curl}\mathbf{u}\times\mathbf{n})$. In 2D, (2.12) reduces to

$$\operatorname{rot}\mathbf{u}=0,\quad\text{and}\quad\mathbf{u}\cdot\mathbf{n}=0, \tag{2.14}$$

where $\operatorname{rot}\mathbf{u}:=\partial_{x_1}u_2-\partial_{x_2}u_1$ for $\mathbf{u}=(u_1,u_2)$.

de Rham complexes with zero BCs. The homogeneous tangential trace $\mathbf{v}\times\mathbf{n}=0$ defines $\mathbf{H}_0(\operatorname{curl})$, and $\mathbf{u}\cdot\mathbf{n}=0$ defines $\mathbf{H}_0(\operatorname{div})$ as the normal trace space. Thus, the physics is embedded in the topology of the complex, not added as external constraints. We define

$$H^1_0:=\Big\{v\in H^1:v=0\text{ on }\partial\Omega\Big\} \tag{2.15a}$$

$$\mathbf{H}_0(\operatorname{curl}):=\{\mathbf{v}\in\mathbf{H}(\operatorname{curl}):\mathbf{v}\times\mathbf{n}=0\text{ on }\partial\Omega\} \tag{2.15b}$$

$$\mathbf{H}_0(\operatorname{div}):=\{\mathbf{v}\in\mathbf{H}(\operatorname{div}):\mathbf{v}\cdot\mathbf{n}=0\text{ on }\partial\Omega\} \tag{2.15c}$$

$$L^2_0:=\Big\{v\in L^2:\int v=0\text{ over }\Omega\Big\} \tag{2.15d}$$

Hence, (2.8a) and (2.8b) with zero BCs become

$$H^1_0\xrightarrow{\operatorname{grad}}\mathbf{H}_0(\operatorname{curl})\xrightarrow{\operatorname{curl}}\mathbf{H}_0(\operatorname{div})\xrightarrow{\operatorname{div}}L^2_0\,, \tag{2.16a}$$

$$H^1_0\xrightarrow{\operatorname{curl}}\mathbf{H}_0(\operatorname{div})\xrightarrow{\operatorname{div}}L^2_0\,. \tag{2.16b}$$

Stokes complexes with zero BCs. Stokes complexes (2.9) and (2.11) with zero BCs turn into

$$H^1_0\xrightarrow{\operatorname{grad}}\mathbf{H}(\operatorname{grad}\operatorname{curl})\cap\mathbf{H}_0(\operatorname{curl})\xrightarrow{\operatorname{curl}}\mathbf{H}^1\cap\mathbf{H}_0(\operatorname{div})\xrightarrow{\operatorname{div}}L^2_0, \tag{2.17a}$$

$$H^2\cap H^1_0\xrightarrow{\operatorname{curl}}\mathbf{H}^1\cap\mathbf{H}_0(\operatorname{div})\xrightarrow{\operatorname{div}}L^2_0, \tag{2.17b}$$

in 3D and 2D, respectively. Exactness of (2.9)–(2.11), on contractible Lipschitz domains Ω with (2.12)–(2.14), eliminates harmonic fields and underpins §3–§4; we state it next.

Lemma 2.2 (Exactness of the Stokes Complex)**.** *The stokes complex with zero homogeneous traces* (2.17a) *is exact over contractible Lipschitz domain* Ω*.*

Proof. To prove exactness it suffices to verify at each node that $\mathcal{R}(d_{r-1}) = \mathcal{N}(d_r)$. The following follows standard arguments; see Girault & Raviart [GR12].

Step 1. Node 1: $\mathcal{N}(\text{grad}) = \{0\}$

$\mathcal{N}(\text{grad}) \subseteq \{0\}$:
If $\alpha \in H_0^1(\Omega)$ and $\nabla\alpha = \mathbf{0}$, then α is constant in Ω; the homogeneous trace gives $\alpha|_{\partial\Omega} = 0$, hence $\alpha \equiv 0$.

$\{0\} \subseteq \mathcal{N}(\text{grad})$:
Trivially, $0 \in H_0^1(\Omega)$ and $\nabla 0 = \mathbf{0}$. Thus $\{0\} \subseteq \mathcal{N}(\nabla)$.

Step 2. Node 2: $\mathcal{R}(\text{grad}) = \mathcal{N}(\text{curl})$

$\mathcal{R}(\text{grad}) \subseteq \mathcal{N}(\text{curl})$:
For $\alpha \in H_0^1(\Omega)$, $\mathbf{v} = \nabla\alpha$ satisfies $\operatorname{curl}\mathbf{v} = \operatorname{curl}(\nabla\alpha) = \mathbf{0}$, hence $\mathbf{v} \in \mathcal{N}(\text{curl})$.

$\mathcal{R}(\text{grad}) \supseteq \mathcal{N}(\text{curl})$:
If $\mathbf{v} \in \mathbf{H}(\operatorname{curl}^2) \cap \mathbf{H}_0(\text{curl})$ and $\operatorname{curl}\mathbf{v} = \mathbf{0}$, contractibility yields $\mathbf{v} = \nabla\alpha$ for some $\alpha \in H^1(\Omega)$. The trace $\mathbf{v} \times \mathbf{n} = \mathbf{0}$ forces $\alpha|_{\partial\Omega}$ to be constant; subtracting that constant gives $\tilde{\alpha} \in H_0^1(\Omega)$ with $\nabla\tilde{\alpha} = \mathbf{v}$.

Step 3. Node 3: $\mathcal{R}(\text{curl}) = \mathcal{N}(\text{div})$

$\mathcal{R}(\text{curl}) \subseteq \mathcal{N}(\text{div})$:
For any $\mathbf{w} \in \mathbf{H}(\operatorname{curl}^2) \cap \mathbf{H}_0(\text{curl})$, $\operatorname{div}(\operatorname{curl}\mathbf{w}) = 0$; hence $\operatorname{curl}\mathbf{w} \in \mathcal{N}(\text{div})$.

$\mathcal{R}(\text{curl}) \supseteq \mathcal{N}(\text{div})$:
If $\mathbf{u} \in \mathbf{H}^1 \cap \mathbf{H}_0(\text{div})$ with $\operatorname{div}\mathbf{u} = 0$, then (de Rham) $\exists\, \mathbf{w} \in \mathbf{H}_0(\text{curl})$ such that $\mathbf{u} = \operatorname{curl}\mathbf{w}$. Elliptic regularity (Girault–Raviart, Thm. 3.9) yields $\mathbf{w} \in H^2(\Omega) \subset \mathbf{H}(\operatorname{curl}^2)$, so indeed $\mathbf{u} \in \mathcal{R}(\text{curl})$.

Step 4. Last node: $\mathcal{R}(\mathrm{div}) = L^2_0(\Omega)$

$\mathcal{R}(\mathrm{div}) \subseteq L^2_0(\Omega)$:
If $\mathbf{u} \in \mathbf{H}^1 \cap \mathbf{H}_0(\mathrm{div})$, then $\int_\Omega \mathrm{div}\,\mathbf{u} = \int_{\partial\Omega} \mathbf{u}\cdot\mathbf{n} = 0$; hence $\mathrm{div}\,\mathbf{u} \in L^2_0(\Omega)$.

$\mathcal{R}(\mathrm{div}) \supseteq L^2_0(\Omega)$:
Given $f \in L^2_0(\Omega)$, solve the Neumann problem $-\Delta\alpha = f$ with $\partial_n\alpha = 0$. By Grisvard (Thm. 3.1.3), $\alpha \in H^3$. Then $\mathbf{u} = \nabla\alpha \in H^2(\Omega) \subset \mathbf{H}^1 \cap \mathbf{H}_0(\mathrm{div})$ and $\mathrm{div}\,\mathbf{u} = f$.

□

Remark 2.3 (Elliptic Regularity)**.** *The need for $C^{2,1}$–boundary regularity is sharp for the elliptic systems in Steps 3-4:*

i) Step 3 ($\mathbf{w}$–regularity): The system $\mathrm{curl}(\mathrm{curl}\,\mathbf{w}) = \mathbf{g}$ *with* $\mathbf{w}\times\mathbf{n} = \mathbf{0}$ *and* $\mathrm{curl}\,\mathbf{w}\times\mathbf{n} = \mathbf{0}$ *is elliptic when $\Omega \in C^{2,1}$. The H^2–regularity follows from the Agmon–Douglis–Nirenberg theory for nonhomogeneous boundary conditions (Girault & Raviart [GR12, Thm. 3.9]).*

ii) Step 4 (α–regularity): The Neumann problem $-\Delta\alpha = f$, $\partial_n\alpha = 0$ is uniformly elliptic. The H^3–regularity requires $\partial\Omega \in C^{2,1}$ to control third derivatives near the boundary (Girault & Raviart [GR12, Thm. 3.1.3]).

Weaker boundaries (e.g., Lipschitz) would yield only H^{1+s} ($s < \frac{1}{2}$), breaking the complex.

Remark 2.4 (On topology and exactness)**.** *Under Assumption* **??**, *the domain Ω is contractible, so its de Rham cohomology is trivial: equivalently $H^k_{\mathrm{dR}}(\Omega) = 0$ for $k \geq 1$. In particular, there are no nontrivial harmonic fields, and the de Rham/Stokes complexes with the homogeneous traces are exact. That is,* curl*–free fields with vanishing tangential trace are gradients,* div*–free fields with vanishing normal trace are curls, and there are no nontrivial harmonic fields. The extension to nontrivial topologies is deferred to future work.*

Quantities of interest. Integral equalities of interest in studying the evolution and structure of the flow in this work are defined as:

$$\text{Energy}: \quad \mathcal{K} := \frac{1}{2}\|\mathbf{u}\|^2, \tag{2.18a}$$

$$\text{Helicity}: \quad \mathcal{H} := \frac{1}{2}(\mathbf{u}, \operatorname{curl}\mathbf{u}), \tag{2.18b}$$

$$\text{Enstrophy}: \quad \mathcal{E} := \frac{1}{2}\|\nabla\mathbf{u}\|^2, \tag{2.18c}$$

$$\text{Palinstrophy}: \quad \mathcal{P} := \frac{1}{2}\|\operatorname{curl}\boldsymbol{\omega}\|^2. \tag{2.18d}$$

Wer ein Warum zum Leben hat, erträgt fast jedes Wie.
He who has a why to live can bear almost any how.

— Friedrich Nietzsche, *Götzen-Dämmerung* (*Twilight of the Idols*), tr. Walter Kaufmann

3

Structure–preserving discretisations

Contents

In this chapter, our objective is to construct an integrator that dissipates energy correctly and yields the appropriate enstrophy behaviour on under–resolved meshes, while remaining implementable in standard FE technology. We begin with a brief review of the current energy– and enstrophy–stable integrators to position the contribution. We then present the AV–FEEC framework and the finite–element complex choices used in the construction. The chapter closes with the proofs of the discrete energy and enstrophy properties we desire.

3.1 Related literature

This brief review isolates the key precedents and locates our contribution among them. We emphasise what we adopt, what we adapt, and what we choose to avoid.

3.1.1 Energy– & enstrophy–stable integrators

Mixed stream function–vorticity discretisations for the incompressible Navier–Stokes equations were first introduced by Liu & E [LE01] in both two and three dimensions. In 2D, this formulation has since been extensively analysed i.e. the convergence study using non-conforming elements by Liu & Shu [LS00], or the more recent review by Cotter [Cot23, Sec. 7.2]; which presents an equivalent reparametrisation to the dual–field velocity–vorticity discretisation proposed by Palha & Gerritsma [PG17]. The finite element spaces used in their constructions are likewise required to satisfy the complex relations discussed in §2. This latter dual–field discretisation was later extended by Zhang et al. [Zha+24] to accommodate general boundary conditions, who also provided an analysis of its structure–preserving properties—mass, energy, enstrophy, and vorticity—and adopted the acronym MEEVC to reflect these. Notably, the MEEVC scheme dissipates an auxiliary enstrophy $\tilde{\mathcal{E}}(\omega) := \frac{1}{2}\|\omega\|^2$, whereas our 2D integrator (3.7) preserves enstrophy on the primal variable $\mathcal{E}(\mathbf{u}) := \frac{1}{2}\|\operatorname{rot}\mathbf{u}\|^2$. We further compare these notions of auxiliary and primal enstrophy preservation in §3.3.3. Zhang et al. [Zha+24, Sec. 5.2] also report stabilisation of their scheme on under–resolved meshes, demonstrated by the roll–up of a shear layer at $\mathrm{Re} = \infty$; against which we compare our 2D integrator in §5.1.

In 3D, Hanot [Han23] recently proposed a one–stage mixed velocity–vorticity integrator, which, in 2D, is equivalent to a reparametrisation of the MEEVC scheme. The distinction lies in the definition of the vorticity field: in our formulation (3.5), $\boldsymbol{\omega}$ is obtained as the $\mathbf{H}(\mathrm{curl})$–projection of $\operatorname{curl}\mathbf{u}$, whereas Hanot defines this projection in the L^2 sense.

3.1.2 GNI via auxiliary variables

We now introduce the auxiliary framework of Andrews & Farrell [AF25], which forms the foundation for the energy– and enstrophy–preserving integrator developed in §3.2. For a full detour please refer to [AF25].

Framework (A–F)

A. *Choose ansatz.* Pick a finite–dimensional spatial trial/test space $\mathbb{U}$ and time–shape spaces (polynomials on each timestep); pose the semidiscrete problem

$$M(u; \dot{u}, v) = F(u; v) \qquad \forall v \in \mathbb{U}.$$

B. *Fix timestep template.* Select a sign–preserving time operator $\mathcal{I}_n$ (e.g. a positive quadrature) and restrict unknowns and tests to the chosen time–polynomial spaces to obtain the discrete timestep problem.

C. *Identify associated tests.* For each quantity Q_p to be conserved/dissipated, find the associated test $w_p(u)$ satisfying

$$Q_p'(u; v) = M(u; v, w_p(u)) \qquad \forall v \in \mathbb{U}.$$

D. *Introduce auxiliary variables (AVs).* For each p define $\widetilde{w}_p$ in the discrete test space by the AV–projection (a Riesz–type solve in time):

$$\mathcal{I}_n\big[M(u; v, \widetilde{w}_p)\big] = \int_{T_n} Q_p'(u; v)\,\mathrm{d}t \qquad \forall v \text{ (discrete tests)}.$$

E. *Modify the RHS.* Replace occurrences of the formal tests $w_p(u)$ in F by the computable AVs $\widetilde{w}_p$, choosing the modified $\widehat{F}$ so that (i) it is linear in the test argument, (ii) it is consistent when $\widetilde{w}_p = w_p(u)$, and (iii) it has the prescribed sign when evaluated at the AVs.

F. *Solve the coupled step & recover one-step balance.* Solve the discrete system for u and the AVs $\{\widetilde{w}_p\}$. By construction

$$Q_p(u_{n+1}) - Q_p(u_n) = \mathcal{I}_n\big[\widehat{F}(u, \{\widetilde{w}_\ell\}; \widetilde{w}_p)\big],$$

so each Q_p is conserved or dissipated according to the sign imposed in Step E (up to quadrature/solver error).

3.2 Structure–preserving discretisation

We construct a FEEC–compatible AV semi–discretisation following §3.1.2. As a baseline, we recall the structure–preserving formulation of Palha & Gerritsma [PG17], which starts from the Lamb form (2.3) and introduces the vorticity as an auxiliary unknown $\boldsymbol{\omega} := \operatorname{curl} \mathbf{u}$. Using the vector identity $\Delta \mathbf{u} = \nabla(\operatorname{div} \mathbf{u}) - \operatorname{curl}(\operatorname{curl} \mathbf{u})$; the viscous term may be left as $\Delta \mathbf{u}$ or, under incompressibility $\operatorname{div} \mathbf{u} = 0$, recast as $\Delta \mathbf{u} = -\operatorname{curl} \boldsymbol{\omega}$. This yields the strong form

$$\dot{\mathbf{u}} = \mathbf{u} \times \boldsymbol{\omega} - \nabla p + \frac{1}{\mathrm{Re}} \Delta \mathbf{u}, \tag{3.1a}$$

$$0 = \operatorname{div} \mathbf{u}, \tag{3.1b}$$

$$\boldsymbol{\omega} = \operatorname{curl} \mathbf{u}. \tag{3.1c}$$

While this scheme is not an instance of the AV framework by Andrews & Farrell [AF25]—the discrete vorticity $\boldsymbol{\omega}$ therein is not a projection of a function of the discrete velocity $\mathbf{u}$, but evolves according to its own coupled equation—we note that the spaces occupied by $\boldsymbol{\omega}$, $\mathbf{u}$, and the pressure p are required to satisfy the same FE complex relations as those identified in §2. To place $\boldsymbol{\omega}$ in the divergence–free space of the de Rham/Stokes complex and avoid second derivatives of $\mathbf{u}$, we reconstruct $\boldsymbol{\omega}$ via a constrained vector Poisson problem (a discrete Leray projection): seek $(\boldsymbol{\omega}, \theta)$ such that $\Delta\boldsymbol{\omega} - \nabla\theta = \Delta(\operatorname{curl} \mathbf{u})$ and $\operatorname{div} \boldsymbol{\omega} = 0$ (with the usual homogeneous traces). This amounts to projecting $\operatorname{curl} \mathbf{u}$ onto $\mathcal{N}(\operatorname{div})$ and is well posed; on smooth fields the constraints force $\boldsymbol{\omega} = \operatorname{curl} \mathbf{u}$ exactly.

$$\dot{\mathbf{u}} = \mathbf{u} \times \boldsymbol{\omega} - \nabla p + \frac{1}{\mathrm{Re}} \Delta \mathbf{u}, \tag{3.2a}$$

$$0 = \operatorname{div} \mathbf{u}, \tag{3.2b}$$

$$\Delta\boldsymbol{\omega} - \nabla\theta = \Delta(\operatorname{curl} \mathbf{u}), \tag{3.2c}$$

$$0 = \operatorname{div} \boldsymbol{\omega}. \tag{3.2d}$$

We next factor the Laplacian through the complex, $\Delta = \operatorname{grad} \operatorname{div} - \operatorname{curl}^2$. Under the constraints $\operatorname{div} \mathbf{u} = \operatorname{div} \boldsymbol{\omega} = 0$, this reduces to $\Delta = -\operatorname{curl}^2$ in both (3.2a) and (3.2c), thereby expressing viscosity through a curl–curl operator on $\mathbf{u}$ and producing the coupled identity $\operatorname{curl}^3 \mathbf{u} = \operatorname{curl}^2 \boldsymbol{\omega} + \nabla\theta$. The resulting strong system (3.3) is algebraically equivalent to the Navier–Stokes equations, but aligned with the FEEC complex, preserving skew–symmetry of advection and paving the way for the discrete energy (and, in two dimensions, enstrophy) balances established in §3.3.

$$\dot{\mathbf{u}} = \mathbf{u} \times \boldsymbol{\omega} - \nabla p - \frac{1}{\mathrm{Re}} \operatorname{curl}^2 \mathbf{u}, \tag{3.3a}$$

$$0 = \operatorname{div} \mathbf{u}, \tag{3.3b}$$

$$\operatorname{curl}^3 \mathbf{u} = \operatorname{curl}^2 \boldsymbol{\omega} + \nabla\theta, \tag{3.3c}$$

$$0 = \operatorname{div} \boldsymbol{\omega}. \tag{3.3d}$$

We next pass (3.3) to an L^2–weak formulation over FEEC–compatible spaces (the discrete Stokes complexes), which yields the structure–preserving semidiscretisations below.

Structure–preserving semidiscretisations

In three spatial dimensions, and using FEEC–compatible spaces forming the discrete Stokes complex

$$\begin{array}{ccccccc} H_0^1 & \xrightarrow{\text{grad}} & \mathbf{H}(\text{curl}^2) \cap \mathbf{H}_0(\text{curl}) & \xrightarrow{\text{curl}} & \mathbf{H}^1 \cap \mathbf{H}_0(\text{div}) & \xrightarrow{\text{div}} & L_0^2 \\ \downarrow & & \downarrow & & \downarrow & & \downarrow \\ \mathbb{Q} & \xrightarrow{\text{grad}} & \mathbb{V} & \xrightarrow{\text{curl}} & \overline{\mathbb{V}} & \xrightarrow{\text{div}} & \overline{\mathbb{Q}} \end{array} \tag{3.4}$$

we seek $(\mathbf{u}, p, \boldsymbol{\omega}, \theta) \in \overline{\mathbb{V}} \times \overline{\mathbb{Q}} \times \mathbb{V} \times \mathbb{Q}$ such that

$$(\dot{\mathbf{u}}, \mathbf{v}) = (\mathbf{u} \times \boldsymbol{\omega}, \mathbf{v}) + (p, \operatorname{div} \mathbf{v}) - \frac{1}{\mathrm{Re}}(\operatorname{curl} \boldsymbol{\omega}, \mathbf{v}), \tag{3.5a}$$

$$0 = (\operatorname{div} \mathbf{u}, q), \tag{3.5b}$$

$$(\operatorname{curl} \boldsymbol{\omega}, \operatorname{curl} \boldsymbol{\chi}) = \left(\operatorname{curl} \mathbf{u}, \operatorname{curl}^2 \boldsymbol{\chi}\right) + (\nabla\theta, \boldsymbol{\chi}), \tag{3.5c}$$

$$0 = (\boldsymbol{\omega}, \nabla\eta), \tag{3.5d}$$

for all $(\mathbf{v}, q, \boldsymbol{\chi}, \eta) \in \overline{\mathbb{V}} \times \overline{\mathbb{Q}} \times \mathbb{V} \times \mathbb{Q}$. In two dimensions, with a discrete Stokes complex

$$\begin{array}{ccccc} H^2 \cap H_0^1 & \xrightarrow{\text{curl}} & \mathbf{H}^1 \cap \mathbf{H}_0(\text{div}) & \xrightarrow{\text{div}} & L_0^2 \\ \downarrow & & \downarrow & & \downarrow \\ \mathbb{U} & \xrightarrow{\text{curl}} & \overline{\mathbb{V}} & \xrightarrow{\text{div}} & \overline{\mathbb{Q}} \end{array} \tag{3.6}$$

we seek $(\mathbf{u}, p, \omega) \in \overline{\mathbb{V}} \times \overline{\mathbb{Q}} \times \mathbb{U}$ such that

$$(\dot{\mathbf{u}}, \mathbf{v}) = (\omega\, \mathbf{u}_\perp, \mathbf{v}) + (p, \operatorname{div} \mathbf{v}) - \frac{1}{\mathrm{Re}}(\operatorname{curl} \omega, \mathbf{v}), \tag{3.7a}$$

$$0 = (\operatorname{div} \mathbf{u}, q), \tag{3.7b}$$

$$(\nabla\omega, \nabla\chi) = -(\operatorname{rot} \mathbf{u}, \Delta\chi), \tag{3.7c}$$

for all $(\mathbf{v}, q, \chi) \in \overline{\mathbb{V}} \times \overline{\mathbb{Q}} \times \mathbb{U}$.

3.3 Structure–preserving properties

Next, in §3.3.1, we establish energy stability in 3D (Theorem 3.1) and 2D (Corollary 3.3). In §3.3.2, Theorem 3.5 (3D) and Corollary 3.7 (2D) establish enstrophy stability. Taken together, these results show that the integrator (3.5)–(3.7), derived from the framework of §3.1.2, is both energy– and enstrophy–stable.

3.3.1 Energy stability

The first structure we consider in the incompressible NS integrator (3.5)–(3.7) is the dissipation (or conservation) of energy $\mathcal{K} = \frac{1}{2}\|\mathbf{u}\|^2$, where $\mathbf{u}$ is the velocity and $\|\cdot\| = \|\cdot\|_{L^2(\Omega)}$ denotes the L^2 norm. This is widely regarded as the most fundamental structure within the Navier–Stokes equations, and is crucial to their analysis (see Temam & Chorin [TC78] and Girault & Raviart [GR12]); the preservation of energy stability, i.e. constructing schemes that preserve the conservation (or dissipation) of energy discretely, is consequently necessary for the design of well–posed numerical integrators; related work is reviewed in §1.1.1.

Theorem 3.1 (Energy stability of the incompressible NS integrator)**.** *When integrating in time using a Gauss method, the incompressible NS integrator* (3.5) *is energy stable, with the discrete analogue of the following dissipation relation* (3.8) *holding across each timestep* T_n*:*

$$\dot{\mathcal{K}} \;=\; -\frac{1}{\mathrm{Re}}\,\|\operatorname{curl}\mathbf{u}\|^2 \;(\leq 0) \tag{3.8}$$

Proof. Energy stability follows by testing (3.5) against $(\mathbf{v}, q, \boldsymbol{\chi}) = (\mathbf{u}, p, \boldsymbol{\psi}) \in \overline{\mathbb{V}} \times \overline{\mathbb{Q}} \times \mathbb{V}$, where $\boldsymbol{\psi} \in \mathbb{V}$ is a vector potential with $\operatorname{curl}\boldsymbol{\psi} = \mathbf{u}$ (unique up to gradients); see Remark 3.2. First, test (3.5a) against $\mathbf{v} = \mathbf{u}$:

$$(\dot{\mathbf{u}}, \mathbf{u}) = (\mathbf{u} \times \boldsymbol{\omega}, \mathbf{u}) + (p, \operatorname{div}\mathbf{u}) - \frac{1}{\mathrm{Re}}\,(\operatorname{curl}\boldsymbol{\omega}, \mathbf{u}). \tag{3.9}$$

The triple product is skew, so $(\mathbf{u} \times \boldsymbol{\omega}, \mathbf{u}) = 0$. Using (3.5b) with $q = p$ gives $(\operatorname{div}\mathbf{u}, p) = 0$. Hence

$$(\dot{\mathbf{u}}, \mathbf{u}) = -\frac{1}{\mathrm{Re}}\,(\operatorname{curl}\boldsymbol{\omega}, \mathbf{u}). \tag{3.10}$$

In (3.5c), take $\boldsymbol{\chi} = \nabla\theta$[1].

$$\begin{array}{ccccccc} H^1_0 & \xrightarrow{\text{grad}} & \mathbf{H}(\operatorname{curl}^2) \cap \mathbf{H}_0(\operatorname{curl}) & \xrightarrow{\text{curl}} & \mathbf{H}^1 \cap \mathbf{H}_0(\operatorname{div}) & \xrightarrow{\text{div}} & L^2_0 \\ \downarrow & & \downarrow & & \downarrow & & \downarrow \\ \mathbb{Q} & \xrightarrow{\text{grad}} & \mathbb{V} & \xrightarrow{\text{curl}} & \overline{\mathbb{V}} & \xrightarrow{\text{div}} & \overline{\mathbb{Q}} \end{array} \tag{3.11}$$

By Lemma 2.2 $\Big(\operatorname{curl}(\operatorname{grad} *) = 0\Big)$,

$$\underbrace{(\operatorname{curl}\boldsymbol{\omega}, \operatorname{curl}\nabla\theta)}_{=0} = \underbrace{(\operatorname{curl}\mathbf{u}, \operatorname{curl}^2\nabla\theta)}_{=0} + (\nabla\theta, \nabla\theta) = \|\nabla\theta\|^2 \;\rightarrow\; \nabla\theta = 0. \tag{3.12}$$

Next, set $\boldsymbol{\chi} = \boldsymbol{\psi}$ in (3.5c). Using $\operatorname{curl}\boldsymbol{\psi} = \mathbf{u}$ and $\nabla\theta = 0$,

[1] With $\theta \in H^1_0(\Omega)$, $\boldsymbol{\chi} = \nabla\theta \in \mathbb{V}$; see (3.11).

$$(\operatorname{curl}\boldsymbol{\omega}, \operatorname{curl}\boldsymbol{\psi}) \;=\; (\operatorname{curl}\mathbf{u}, \operatorname{curl}\mathbf{u}). \tag{3.13}$$

Thus, (3.10) with $(\dot{\mathbf{u}}, \mathbf{u}) = \frac{1}{2}\frac{\mathrm{d}}{\mathrm{d}x}\|\mathbf{u}\|^2$ gives the correct $\mathbf{H}(\mathrm{curl})$–seminorm dissipation

$$\dot{\mathcal{K}} \;=\; -\frac{1}{\mathrm{Re}}(\operatorname{curl}\mathbf{u}, \operatorname{curl}\mathbf{u}) \;=\; -\frac{1}{\mathrm{Re}}\|\operatorname{curl}\mathbf{u}\|^2. \tag{3.14}$$

□

In the Euler limit $\mathrm{Re} = \infty$, Equation 3.8 reduces to $\dot{\mathcal{K}} = 0$, i.e. the discrete energy is conserved.

Remark 3.2 (Existence and uniqueness of a stream function $\boldsymbol{\psi}$)**.** *We justify the existence of $\boldsymbol{\psi} \in \mathbb{V}$ such that $\operatorname{curl}\boldsymbol{\psi} = \mathbf{u}$ as follows:*
Set $p = \operatorname{div}\mathbf{u}$ in (3.5b); this gives $(\operatorname{div}\mathbf{u}, \operatorname{div}\mathbf{u}) = 0$, hence $\operatorname{div}\mathbf{u} = 0$.

$$\begin{array}{ccccccc}
H_0^1 & \xrightarrow{\text{grad}} & \mathbf{H}(\mathrm{curl}^2)\cap\mathbf{H}_0(\mathrm{curl}) & \xrightarrow{\text{curl}} & \mathbf{H}^1\cap\mathbf{H}_0(\mathrm{div}) & \xrightarrow{\text{div}} & L_0^2 \\
\downarrow & & \downarrow & & \downarrow & & \downarrow \\
\mathbb{Q} & \xrightarrow{\text{grad}} & \mathbb{V} & \xrightarrow{\text{curl}} & \overline{\mathbb{V}} & \xrightarrow{\text{div}} & \overline{\mathbb{Q}}
\end{array} \tag{3.15}$$

On a contractible domain and under exactness of the discrete Stokes complex (Lemma 2.2), $\mathcal{N}(\operatorname{div}) = \mathcal{R}(\operatorname{curl})$, there exists $\boldsymbol{\psi} \in \mathbb{V}$ with $\operatorname{curl}\boldsymbol{\psi} = \mathbf{u}$.

$$\begin{array}{ccccccc}
H_0^1 & \xrightarrow{\text{grad}} & \mathbf{H}(\mathrm{curl}^2)\cap\mathbf{H}_0(\mathrm{curl}) & \xrightarrow{\text{curl}} & \mathbf{H}^1\cap\mathbf{H}_0(\mathrm{div}) & \xrightarrow{\text{div}} & L_0^2 \\
\downarrow & & \downarrow & & \downarrow & & \downarrow \\
\mathbb{Q} & \xrightarrow{\text{grad}} & \mathbb{V} & \xrightarrow{\text{curl}} & \overline{\mathbb{V}} & \xrightarrow{\text{div}} & \overline{\mathbb{Q}}
\end{array} \tag{3.16}$$

Moreover $\mathcal{N}(\operatorname{curl}) = \mathcal{R}(\operatorname{grad})$, so $\boldsymbol{\psi}$ is determined modulo gradients (equivalently, it is unique in the quotient $\mathbb{V}/\mathcal{R}(\operatorname{grad})$). To fix a canonical representative, impose the gradient–orthogonality (coexact) condition $(\boldsymbol{\psi}, \nabla q) = 0$ for all $q \in \mathbb{Q}$, which selects a unique $\boldsymbol{\psi}$ in the affine class $\boldsymbol{\psi} + \mathcal{R}(\operatorname{grad})$. (Alternative normalisations such as $\operatorname{div}\boldsymbol{\psi} = 0$ may be used, depending on the BCs.)

Corollary 3.3 (2D Energy stability)**.** *In 2D, recalling $\operatorname{rot}\mathbf{u} := \partial_{x_1}u_2 - \partial_{x_2}u_1$ and $\operatorname{curl}\psi := (\partial_{x_2}\psi, -\partial_{x_1}\psi)$; the 2D scheme (3.7) satisfies*

$$\dot{\mathcal{K}} \;=\; -\frac{1}{\mathrm{Re}}\|\operatorname{rot}\mathbf{u}\|^2 \;\; (\leq 0). \tag{3.17}$$

Proof. In 2D, $\operatorname{rot} : \mathbf{H}^1 \to L^2$ (vector $\to$ scalar) and $\operatorname{curl} : H^2 \to \mathbf{H}^1$ (scalar $\to$ vector). The proof repeats the verbatim in Theorem 3.1, with curl replaced by rot when

acting on a vector field, and by the 2D curl when acting on a vector potential $\boldsymbol{\psi}$. Analogous to Remark 3.2, we prove the existence of a scalar stream function ψ using Lemma 2.2.

(i) Test (3.7a) with $q = \operatorname{div} \mathbf{u}$; admissibility of this choice follows from the 2D Stokes subcomplex (3.18). One gets $\operatorname{div} \mathbf{u} = 0$.

$$\begin{array}{ccccc} H^2 \cap H_0^1 & \xrightarrow{\text{curl}} & \mathbf{H}^1 \cap \mathbf{H}_0(\text{div}) & \xrightarrow{\text{div}} & L_0^2 \\ \downarrow & & \downarrow & & \downarrow \\ \mathbb{U} & \xrightarrow{\text{curl}} & \overline{\mathbb{V}} & \xrightarrow{\text{div}} & \overline{\mathbb{Q}} \end{array} \tag{3.18}$$

(ii) Lemma 2.2 yields $\mathcal{N}(\text{div}) = \mathcal{R}(\text{curl})$. Since $\operatorname{div} \mathbf{u} = 0$, there exists $\psi \in H^2 \cap H_0^1$ with $\operatorname{curl} \psi = \mathbf{u}$; see (3.19).

$$\begin{array}{ccccc} H^2 \cap H_0^1 & \xrightarrow{\text{curl}} & \mathbf{H}^1 \cap \mathbf{H}_0(\text{div}) & \xrightarrow{\text{div}} & L_0^2 \\ \downarrow & & \downarrow & & \downarrow \\ \mathbb{U} & \xrightarrow{\text{curl}} & \overline{\mathbb{V}} & \xrightarrow{\text{div}} & \overline{\mathbb{Q}} \end{array} \tag{3.19}$$

Since $\psi \in H_0^1$, the only admissible constant is 0, therefore ψ is unique (with other BCs one gets uniqueness modulo constants).

(iii) With $\operatorname{div} \mathbf{u} = 0$ and $\mathbf{u} = \operatorname{curl} \psi$, the algebra in Theorem 3.1 carries over: the convective term is L^2–skew, since $(\omega\, \mathbf{u}_\perp, \mathbf{u}) = 0$. The pressure term vanishes by *(i)*, and the viscosity gives

$$\dot{\mathcal{K}} = -\frac{1}{\mathrm{Re}} (\operatorname{curl} \boldsymbol{\omega}, \mathbf{u}) = -\frac{1}{\mathrm{Re}} (\operatorname{rot} \mathbf{u}, \operatorname{rot} \mathbf{u}) = -\frac{1}{\mathrm{Re}} \| \operatorname{rot} \mathbf{u} \|^2. \tag{3.20}$$

□

The energy balance (3.8) now yields the a priori energy estimates stated in Lemma 3.4.

Lemma 3.4 (A priori estimates from energy stability)**.** *Under Assumption 2.1, if (3.8) holds, then for every $T > 0$,*

$$\sup_{t \geq 0} \|\mathbf{u}\|^2 \;\leq\; \|\mathbf{u}(0)\|^2, \qquad \int_0^\infty \|\nabla \mathbf{u}\|^2 \;\leq\; \frac{\mathrm{Re}}{2} \|\mathbf{u}(0)\|^2. \tag{3.21}$$

Proof. Integrate (3.8) on $[0,t]$ to obtain the exact balance

$$\mathcal{K}(t) \;+\; \frac{1}{\mathrm{Re}}\int_0^t \|\operatorname{curl}\mathbf{u}(s)\|^2\,\mathrm{d}s \;=\; \mathcal{K}(0), \tag{3.22a}$$

$$\xrightarrow{\mathcal{K}(t)\geq 0} \quad \sup_{[0,T]}\|\mathbf{u}\|^2 \leq \|\mathbf{u}(0)\|^2, \quad \int_0^T \|\operatorname{curl}\mathbf{u}\|^2\,\mathrm{d}t \;\leq\; \frac{\mathrm{Re}}{2}\|\mathbf{u}(0)\|^2. \tag{3.22b}$$

Under Assumption 2.1 the standard identity $\|\nabla\mathbf{u}\|^2 = \|\operatorname{curl}\mathbf{u}\|^2 + \|\operatorname{div}\mathbf{u}\|^2$ holds, and with $\operatorname{div}\mathbf{u}=0$ this gives $\|\operatorname{curl}\mathbf{u}\| = \|\nabla\mathbf{u}\|$. Substituting yields the second estimate in (3.21). The bounds in (1.2) follow by letting $T\to\infty$. □

As previously discussed in §1.1.2, the second estimate in (3.21) scales with Re. On finite–dimensional spaces, norm equivalence already lifts the L^2 bound to an $\mathbf{H}^1$ bound up to a mesh–dependent constant; thus, unless the Re–dependent factor is small, the estimate does not meaningfully constrain $\|\nabla\mathbf{u}\|$. In particular, for under–resolved regimes ($h^2\mathrm{Re}\gg 1$) the bound becomes ineffective, and spurious oscillations can appear in simulations of $\mathbf{H}^1$–conforming discretisations; see Figure 5.3.

3.3.2 Enstrophy stability

Energy stability alone does not provide a robust $\mathbf{H}^1$ control at high Re (cf. Lemma 3.4). To obtain an Re–independent bound on $\|\nabla\mathbf{u}\|$ in two dimensions, we turn to the enstrophy structure. In this subsection we establish the enstrophy evolution law for the 3D scheme (Theorem 3.5) and its 2D dissipative corollary (Corollary 3.7), and then derive the associated a priori estimates for $\|\nabla\mathbf{u}\|$ and $\|\Delta\mathbf{u}\|$.

Theorem 3.5 (Enstrophy stability of the incompressible NS integrator)**.** *When integrating in time using a Gauss method, the incompressible NS integrator* (3.5) *is enstrophy stable, with the discrete analogue of the following relation holding across each timestep $T_n=[t_n,t_{n+1}]$:*

$$\dot{\mathcal{E}} \;=\; (\mathbf{u}\times\boldsymbol{\omega},\operatorname{curl}\boldsymbol{\omega}) - \frac{1}{\mathrm{Re}}\|\operatorname{curl}\boldsymbol{\omega}\|^2. \tag{3.23}$$

Proof. To derive enstrophy stability, we test (3.5) against $(\mathbf{v},\boldsymbol{\chi}) = (\operatorname{curl}\boldsymbol{\omega},\dot{\psi}) \in \overline{\mathbb{V}}\times\mathbb{V}$. First, set $\boldsymbol{\chi}=\nabla\theta$ in (3.5c). By Lemma 2.2, $\operatorname{curl}(\operatorname{grad}*)=0$ and $\operatorname{curl}^2(\operatorname{grad}*)=0$; we obtain $\nabla\theta=0$; exactly as in Equation 3.12. Subsequently, take $\boldsymbol{\chi}=\boldsymbol{\omega}$ in (3.5c):

$$\|\operatorname{curl}\boldsymbol{\omega}\|^2 = (\operatorname{curl}\mathbf{u},\operatorname{curl}^2\boldsymbol{\omega}). \tag{3.24}$$

Next, set $\mathbf{v}=\operatorname{curl}\boldsymbol{\omega}$ in (3.5a). This choice is admissible because $\operatorname{curl}\boldsymbol{\omega}\in\mathbb{V}$; see (3.16). Using $\operatorname{div}(\operatorname{curl}\boldsymbol{\omega})=0$ the pressure term drops out and we get

$$(\dot{\mathbf{u}},\operatorname{curl}\boldsymbol{\omega}) = (\mathbf{u}\times\boldsymbol{\omega},\operatorname{curl}\boldsymbol{\omega}) - \frac{1}{\mathrm{Re}}\|\operatorname{curl}\boldsymbol{\omega}\|^2. \tag{3.25}$$

Lastly, set $\boldsymbol{\chi} = \dot{\boldsymbol{\psi}}$ in (3.5c). With $\nabla\theta = 0$,

$$(\operatorname{curl}\boldsymbol{\omega}, \operatorname{curl}\dot{\boldsymbol{\psi}}) = (\operatorname{curl}\mathbf{u}, \operatorname{curl}^2\dot{\boldsymbol{\psi}}). \tag{3.26}$$

Differentiating $\operatorname{curl}\boldsymbol{\psi} = \mathbf{u}$ in time gives $\operatorname{curl}\dot{\boldsymbol{\psi}} = \dot{\mathbf{u}}$; hence (3.26) yields

$$(\operatorname{curl}\boldsymbol{\omega}, \dot{\mathbf{u}}) = \underbrace{(\operatorname{curl}\mathbf{u}, \operatorname{curl}\dot{\mathbf{u}})}_{\frac{\mathrm{d}}{\mathrm{d}t}\frac{1}{2}\|\operatorname{curl}u\|^2} = \dot{\mathcal{E}}. \tag{3.27}$$

Combining (3.25) and (3.27) gives

$$\dot{\mathcal{E}} = (\mathbf{u}\times\boldsymbol{\omega}, \operatorname{curl}\boldsymbol{\omega}) - \frac{1}{\mathrm{Re}}\|\operatorname{curl}\boldsymbol{\omega}\|^2. \tag{3.28}$$

□

One may rewrite Equation 3.28. Using $\operatorname{curl}\boldsymbol{\omega} = \operatorname{curl}(\operatorname{curl}\mathbf{u}) = \nabla(\operatorname{div}\mathbf{u}) - \Delta\mathbf{u} = -\Delta\mathbf{u}$ (since $\operatorname{div}\mathbf{u} = 0$), the boundary traces (2.12), and standard identities such as $(\mathbf{a}\times\mathbf{b})\cdot\mathbf{c} = \mathbf{a}\cdot(\mathbf{b}\times\mathbf{c})$ together with $\boldsymbol{\omega}\times(\operatorname{curl}\boldsymbol{\omega}) = \nabla\left(\frac{1}{2}|\boldsymbol{\omega}|^2\right) - (\boldsymbol{\omega}\cdot\nabla)\boldsymbol{\omega}$, one finds that

$$(\mathbf{u}\times\boldsymbol{\omega}, \operatorname{curl}\boldsymbol{\omega}) \;=\; -\int_\Omega \mathbf{u}\cdot(\boldsymbol{\omega}\cdot\nabla)\boldsymbol{\omega}\,\mathrm{d}\mathbf{x}.$$

Inserting this identity and $\|\operatorname{curl}\boldsymbol{\omega}\|^2 = \|\Delta\mathbf{u}\|^2$ into (3.28) gives

$$\dot{\mathcal{E}} = -\int_\Omega \mathbf{u}\cdot(\boldsymbol{\omega}\cdot\nabla)\boldsymbol{\omega}\,\mathrm{d}\mathbf{x} - \frac{1}{\mathrm{Re}}\|\Delta\mathbf{u}\|^2. \tag{3.29}$$

Remark 3.6 (Geometric interpretation of the convective contribution)**.** *Denote* $\boldsymbol{\omega} = \operatorname{curl}\mathbf{u}$ *and decompose it as* $\boldsymbol{\omega} = |\boldsymbol{\omega}|\,\boldsymbol{\xi}$ *on the set* $\{|\boldsymbol{\omega}| > 0\}$*, with* $\boldsymbol{\xi} = \boldsymbol{\omega}/|\boldsymbol{\omega}|$ *the unit vortex–line direction. The integrand* $\mathbf{u}\cdot(\boldsymbol{\omega}\cdot\nabla)\boldsymbol{\omega}$ *in* (3.29) *can be rewritten using*

$$(\boldsymbol{\omega}\cdot\nabla)\boldsymbol{\omega} \;=\; |\boldsymbol{\omega}|^2\,\underbrace{(\boldsymbol{\xi}\cdot\nabla)\boldsymbol{\xi}}_{\boldsymbol{\kappa}} + |\boldsymbol{\omega}|\,(\boldsymbol{\xi}\cdot\nabla|\boldsymbol{\omega}|)\,\boldsymbol{\xi}. \tag{3.30}$$

$\boldsymbol{\kappa} = (\boldsymbol{\xi}\cdot\nabla)\boldsymbol{\xi}$ *is the curvature of the vortex–line field*[a]*: it measures how rapidly the unit direction* $\boldsymbol{\xi}$ *turns along itself and thus encodes the bending and tilting of vortex lines. When* $\boldsymbol{\xi}$ *is spatially constant (straight vortex lines), this curvature vanishes and the convective contribution to* (3.29) *disappears. In general, the term* $|\boldsymbol{\omega}|^2\,(\boldsymbol{\xi}\cdot\nabla)\boldsymbol{\xi}$ *captures the effect of vortex–line curvature, while the second term* $|\boldsymbol{\omega}|\,(\boldsymbol{\xi}\cdot\nabla|\boldsymbol{\omega}|)\,\boldsymbol{\xi}$ *accounts for changes in the vorticity magnitude along the lines. Enstrophy can thus increase or decrease depending on how the flow* $\mathbf{u}$ *aligns with these curvature and stretching effects: curved vortex lines tend to destabilise enstrophy, whereas dissipative mechanisms progressively straighten and smooth the vortex field; we show this numerically in §5.3.*

[a] $\boldsymbol{\kappa} = \frac{1}{\mathrm{R}}$: Frenet–Serret curvature when restricted to a single line with radius R.

Corollary 3.7 (2D Enstrophy stability)**.** *In 2D, vortex stretching is absent. With* $\mathbf{u}_\perp = (\mathrm{u}_2, -\mathrm{u}_1)$, $\operatorname{curl}\omega = \nabla\omega \times \mathbf{k} = (\partial_y\omega, -\partial_x\omega)$, *and (for* $\operatorname{div}\mathbf{u} = 0$*)* $\operatorname{curl}\boldsymbol{\omega} = -\Delta\mathbf{u}$ *(via the 3D embedding); one obtains enstrophy dissipation given by the* H^2*–seminorm:*

$$\dot{\mathcal{E}} = -\frac{1}{\mathrm{Re}}\|\Delta\mathbf{u}\|^2. \tag{3.31}$$

Proof. There are two equivalent ways to show (3.31).

i) An algebraic proof: recall $\mathbf{u}_\perp := (u_2, -u_1)$ and $\operatorname{curl}\omega := (\partial_y\omega, -\partial_x\omega)$. Then

$$\begin{aligned}(\mathbf{u}\times\boldsymbol{\omega}, \operatorname{curl}\boldsymbol{\omega}) &= \int_\Omega (\mathbf{u}\times\omega\mathbf{k})\cdot(\partial_y\omega, \partial_x\omega, 0)\,\mathrm{d}\mathbf{x} \overset{*}{=} \int_\Omega \omega\,\mathbf{u}_\perp\cdot(\operatorname{curl}\omega)\,\mathrm{d}\mathbf{x}\\ &= \int_\Omega \omega\,\mathbf{u}\cdot\nabla\omega\,\mathrm{d}\mathbf{x} = \tfrac{1}{2}\int_\Omega \mathbf{u}\cdot\nabla(\omega^2)\,\mathrm{d}\mathbf{x} = 0,\end{aligned} \tag{3.32}$$

where $(*)$ uses $(u_1, u_2, 0)\times(0, 0, \omega) = \omega(u_2, -u_1, 0)$. The last line follows from the identity $\mathbf{u}_\perp\cdot\operatorname{curl}\omega = \mathbf{u}\cdot\nabla\omega$, incompressibility $\operatorname{div}\mathbf{u} = 0$, and the standing BCs ($\mathbf{u}\cdot\mathbf{n} = 0$). With $\operatorname{curl}\boldsymbol{\omega} = -\Delta\mathbf{u}$, (3.28) reduces to (3.31).

ii) Next, in line with Remark 3.6; write $\boldsymbol{\omega} := \omega\,\mathbf{k}$ and $\boldsymbol{\xi} := \mathbf{k}$, therefore $(\boldsymbol{\xi}\cdot\nabla) \equiv \partial_z$, $\boldsymbol{\kappa} := (\boldsymbol{\xi}\cdot\nabla)\boldsymbol{\xi} = 0$, and $\partial_z|\boldsymbol{\omega}| = 0$. Using (3.30) and $\mathbf{u}\cdot\boldsymbol{\xi} = 0$, we obtain $\mathbf{u}\cdot(\boldsymbol{\omega}\cdot\nabla)\boldsymbol{\omega} = 0$ pointwise. Hence the convective term in (3.28) vanishes. With $\operatorname{curl}\omega = \nabla\omega\times\mathbf{k}$ and $\operatorname{div}\mathbf{u} = 0$ giving $\operatorname{curl}\boldsymbol{\omega} = -\Delta\mathbf{u}$, (3.28) reduces to (3.31). In short, the vortex lines are straight; thus, the convective contribution disappears, and only dissipation remains.

□

Equation 3.31 clearly implies discrete enstrophy conservation in the inviscid limit $\mathrm{Re}\to\infty$. Furthermore, The 2D enstrophy balance (3.31) yields the a priori estimates announced in §1.1.2.

Lemma 3.8 (A priori estimates from enstrophy stability)**.** *Under Assumption 2.1 in* $d = 2$*, if* (3.31) *holds, then for every* $T > 0$*,*

$$\sup_{t\geq 0}\|\nabla\mathbf{u}\|^2 \;\leq\; \|\nabla\mathbf{u}(0)\|^2, \qquad \int_0^\infty \|\Delta\mathbf{u}\|^2 \;\leq\; \frac{\mathrm{Re}}{2}\|\nabla\mathbf{u}(0)\|^2. \tag{3.33}$$

Proof. Similar to Lemma 3.4, integrate (3.31) on $[0, t]$:

$$\mathcal{E}(t) + \frac{1}{\mathrm{Re}}\int_0^t \|\Delta\mathbf{u}(s)\|^2\,\mathrm{d}s = \mathcal{E}(0), \tag{3.34a}$$

$$\xrightarrow{\mathcal{E}(t)\geq 0} \quad \sup_{t\in[0,T]}\|\nabla\mathbf{u}\|^2 \leq \|\nabla\mathbf{u}(0)\|^2, \qquad \int_0^T \|\Delta\mathbf{u}(t)\|^2\,\mathrm{d}t \leq \frac{\mathrm{Re}}{2}\|\nabla\mathbf{u}(0)\|^2. \tag{3.34b}$$

Last line follows from $\mathcal{E}(0) = \frac{1}{2}\|\nabla\mathbf{u}(0)\|^2$; and Equation 3.33 results upon $T\to\infty$. □

Thus, enstrophy stability supplies the Re–robust $\mathbf{H}^1$ control that energy stability alone cannot provide, together with an $\mathbf{H}^2$–in–time bound scaled by the Reynolds number Re. This mechanism underlies the improved robustness of our integrator on under–resolved 2D meshes; we document the effect numerically in §5.

3.3.3 What exactly is being dissipated?

With the energy and enstrophy balances established in §3.3.1–§3.3.2, we now ask what the scheme is *actually* dissipating in practice, and how this choice compares with the dual–field velocity–vorticity discretisations prominent in the literature; see §3.1.1. This discussion also prepares the ground for the numerical comparison in §5.

A mixed velocity–vorticity formulation. Equation 3.35 in two dimensions[2] yields the mixed velocity–vorticity form

$$\dot{\mathbf{u}} = \mathbf{u} \times \omega \mathbf{k} - \nabla p - \frac{1}{\mathrm{Re}} \operatorname{curl} \omega, \tag{3.35a}$$

$$0 = \operatorname{div} \mathbf{u}, \tag{3.35b}$$

$$\omega = \operatorname{rot} \mathbf{u}. \tag{3.35c}$$

We pass (3.35) to an L^2–based weak formulation in FEEC–compatible spaces; in 2D with a discrete de Rham complex of reduced regularity,

$$\begin{array}{ccccc} H^1_0 & \xrightarrow{\operatorname{curl}} & \mathbf{H}_0(\operatorname{div}) & \xrightarrow{\operatorname{div}} & L^2_0 \\ \downarrow & & \downarrow & & \downarrow \\ \mathbb{U} & \xrightarrow{\operatorname{curl}} & \overline{\mathbb{V}} & \xrightarrow{\operatorname{div}} & \overline{\mathbb{Q}} \end{array} \tag{3.36}$$

we seek $(\mathbf{u}, \omega, p) \in \overline{\mathbb{V}} \times \mathbb{U} \times \overline{\mathbb{Q}}$ such that

$$(\dot{\mathbf{u}}, \mathbf{v}) = (\omega \mathbf{k} \times \mathbf{u}, \mathbf{v}) \; - \; (p, \operatorname{div} \mathbf{v}) \; - \; \frac{1}{\mathrm{Re}} (\operatorname{curl} \omega, \mathbf{v}), \tag{3.37a}$$

$$0 = (\operatorname{div} \mathbf{u}, q), \tag{3.37b}$$

$$(\omega, \chi) = (\operatorname{rot} \mathbf{u}, \chi). \tag{3.37c}$$

for all $(\mathbf{v}, \chi, q) \in \overline{\mathbb{V}} \times \mathbb{U} \times \overline{\mathbb{Q}}$. Up to notation, the weak form (3.37) is precisely the MEEVC formulation [PG17; Zha+24] discussed in §3.2. Under Assumption 2.1, the classical L^2 balances follow directly from (3.37): testing (3.37a) with $\mathbf{v} = \mathbf{u}$ recovers the energy law, identical to (3.8); while in two dimensions, testing (3.37a) with $\mathbf{v} = \operatorname{curl} \omega$ gives the enstrophy relation (3.38).

[2] The study is carried out in two dimensions, where enstrophy has direct physical relevance.

$$\frac{1}{2}\frac{\mathrm{d}}{\mathrm{d}t}\|\mathbf{u}\|^2 = -\frac{1}{\mathrm{Re}}\|\omega\|^2, \qquad \frac{1}{2}\frac{\mathrm{d}}{\mathrm{d}t}\|\omega\|^2 = -\frac{1}{\mathrm{Re}}\|\operatorname{curl}\omega\|^2. \tag{3.38}$$

Primal vs. auxiliary dissipation. Our AV–FEEC scheme (3.5)–(3.7) dissipates enstrophy in the *primal* variable $\frac{1}{2}\|\operatorname{curl}\mathbf{u}\|^2$ (cf. §3.3.2), whereas MEEVC formulations emphasise dissipation of the *auxiliary* enstrophy $\frac{1}{2}\|\boldsymbol{\omega}\|^2$. Do these lead to different stabilising effects, or are they merely two faces of the same coin?

Proposition 3.9 (Equivalence of the two enstrophy dissipated functionals)**.** *Since* $\operatorname{div}(\operatorname{curl}\mathbf{u}) = 0$ *and* $\operatorname{curl}\mathbf{u} \in L^2$*, the field* $\operatorname{curl}\mathbf{u}$ *belongs to* $\mathbf{H}(\operatorname{div})$*. Thus, if in* (3.38) *we set* $\boldsymbol{\omega} := \operatorname{curl}\mathbf{u}$*, then* (3.38) *looks exactly the same as* (3.31)*; in both cases the stabilisation is the norm of*

$$\tfrac{1}{2}\|\boldsymbol{\omega}\|^2_{L^2(\Omega)} \;=\; \tfrac{1}{2}\|\operatorname{curl}\mathbf{u}\|^2_{L^2(\Omega)}. \tag{3.39}$$

However, despite this equivalence in norms, there is a fundamental difference in the admissible space: (3.38) *insists on defining* $\boldsymbol{\omega}$ *as the curl of an* H^1 *finite–element function* $\mathbf{u}$*, whereas* (3.31) *only requires* $\boldsymbol{\omega}$ *to be an* $\mathbf{H}(\operatorname{div})$*–conforming approximation. In particular, as long as* $\mathbf{u}$ *is drawn from an* H^1 *finite–element subspace, the two are essentially the same; the only distinction is that* (3.31) *does not require* $\boldsymbol{\omega}$ *to be of the form* $\operatorname{curl}\mathbf{u}$*.*

In short, the dissipated *functionals* agree $\frac{1}{2}\|\boldsymbol{\omega}\|^2_{L^2(\Omega)} = \frac{1}{2}\|\operatorname{curl}\mathbf{u}\|^2_{L^2(\Omega)}$, while differences—when present—stem from admissible spaces and domain regularity.

Remark 3.10 (Domain regularity and where a difference may appear)**.** *On domains with smooth boundary or on convex polyhedra, one should not expect a large difference between the two forms of stabilisation. On nonconvex polyhedra, however, the set* $\{\mathbf{v} \in [L^2(\Omega)]^d : \mathbf{v} \in \mathbf{H}(\operatorname{curl}) \cap \mathbf{H}(\operatorname{div})\}$ *is strictly larger than* $[H^1]^d$*: for example, Maxwell solutions may lie in* $\mathbf{H}(\operatorname{curl}) \cap \mathbf{H}(\operatorname{div})$ *without belonging to* H^1*. In such a case, an* H^1*–conforming sequence* $\mathbf{u}$ *cannot converge to a limit outside* H^1*, whereas an* $\mathbf{H}(\operatorname{div})$*–conforming* $\boldsymbol{\omega}$ *can still approximate the target; in this sense* (3.31) *is a priori more general than* (3.38)*. By the Gaffney–Friedrichs result* [Gaf55]*,* $[H^1_0]^d = \mathbf{H}_0(\operatorname{curl}) \cap \mathbf{H}_0(\operatorname{div})$ *with equivalent norms on smooth or convex polyhedral domains, but this equality fails on nonconvex polyhedra (Costabel & Dauge [CD00]). We therefore do not propose any rigorous global ordering of the two approaches; any advantage is likely domain– and problem–dependent. Numerical experiments could confirm this; yet such domains lie outside our present setting (see §4.1.1).*

We return to this comparison in §5, where side–by–side experiments on under–resolved meshes quantify the stabilisation afforded by each scheme and show a practical distinction, with our discretisation achieving exact enstrophy conservation in contrast to the MEEVC scheme.

"We shape our tools and thereafter our tools shape us."

— Marshall McLuhan

4

Implementation

Contents

The aim of this chapter is pragmatic: to turn the structure–preserving formulations (3.5)–(3.7) of §3 into executable solvers. The difficulty is architectural rather than algebraic: the semi–discrete schemes that conserve (or dissipate, for finite Re) the relevant quantities of interest are most naturally posed on enhanced regularity FE complexes—discrete Stokes complexes—that are rarely available off the shelf in mainstream FE software. We therefore develop two implementation routes that retain the energy–enstrophy structure proved in §3 while respecting current software limitations. Section 4.1 highlights practical limitations (with `Firedrake` as a running example). Section 4.3 then builds a conforming workaround in 3D and 2D and tracks its inherited stability properties, and §4.2 presents an interior–penalty alternative together with the associated broken energy–enstrophy identities. This closes the gap between analysis and the numerical study in §5.

4.1 Related literature

The conforming schemes derived in §3 presuppose knowledge of—and access to—FE Stokes complexes. We now turn to a brisk tour of the toolchain: which discrete finite–element spaces exist off the shelf, which do not, and how these facts shape our implementation path.

4.1.1 `Firedrake` limitations

This work was implemented in `Firedrake` [Ham+23], which is widely adopted within the Oxford finite–element community, enabling collaboration and support during this study. In `Firedrake` and other publicly available FE software—i.e. `GetFEM++` [RP20], `FreeFEM++` [Hec12] and `FEniCS` [Aln+15]—standard de Rham complexes with $H^1/\mathbf{H}(\mathrm{curl})/\mathbf{H}(\mathrm{div})$ conformity are widely available, whereas enhanced–regularity Stokes complexes (e.g. $\mathbf{H}(\mathrm{curl}^2) \cap \mathbf{H}_0(\mathrm{curl})$ and $\mathbf{H}^1 \cap \mathbf{H}_0(\mathrm{div})$ in 3D, or H^2 in 2D) are not currently exposed as native elements. As a consequence, direct assembly of (3.5)–(3.7) is impractical. This motivates the interior–penalty alternative in §4.2 and the conforming workaround in §4.3, both designed to preserve the energy–enstrophy structure within the available spaces.

2D The Scott–Vogelius (SV) [SV85a; SV85b] complex (as considered in §3) takes $\mathbb{U}$ to be the Morgan–Scott ($\mathbb{MS}$) [MS75] space, which is not implemented in mainstream FE software. Over Alfeld–split [Alf84] (or barycentrically refined; see Figure 4.1) meshes, the $\mathbb{MS}$ space becomes the Hsieh–Clough–Tocher ($\mathbb{HCT}$) [CT65] space; the $\mathbb{HCT}$ space, on the other hand, is relatively well–supported, e.g. in `Firedrake` through `FIAT` (see Brubeck & Kirby [BK25]).

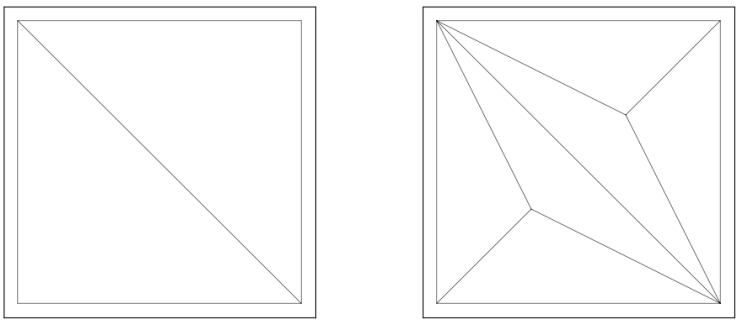

Figure 4.1: Comparison between the standard mesh (left) and the Alfeld–split (barycentrically refined) mesh (right) used in this work.

3D Finite element (FE) Stokes complexes in three dimensions remain relatively rare. The first FE Stokes complexes on general tetrahedral meshes were introduced by Neilan [Nei15] and were later extended by Chen & Huang [CH24] to de Rham complexes of arbitrary smoothness. For such complexes on Alfeld–split meshes, see Fu, Guzmán & Neilan [FGN20] and Hu, Zhang & Zhang [HZZ22]. The Guzmán–Neilan [GN18] $\mathbf{H}^1$–conforming element—used in certain such complexes on Alfeld splits—is available in `Firedrake`; however, to the best of our knowledge, none of the proposed $\mathbf{H}(\operatorname{grad}\operatorname{curl})$– or $\mathbf{H}(\operatorname{curl}^2)$–conforming spaces are currently supported in any publicly available FE software.

For biharmonic–type equations, Ainsworth & Parker [AP24a; AP24b] introduce reparametrised systems that allow one to employ H^2–conforming scalar FEs in effect, while implementing only elements with at most H^1 conformity. Our schemes (3.5)–(3.7) closely mirror—and are strongly inspired by—their construction.

4.2 Nonconforming interior–penalty formulation

In what follows, we assume access only to a discrete de Rham complex; see (4.1) (cd. Figure 2.1). Hence, $\mathbf{u} \in \mathbf{H}_0(\operatorname{div})$ but not necessarily in $\mathbf{H}(\operatorname{curl})$ (cf. (3.5)). The divergence–free constraint is therefore standard (3.5b), but the $\mathbf{H}(\operatorname{curl})$ pairing $(\operatorname{curl}\mathbf{u}, \operatorname{curl}^2\boldsymbol{\chi})$ that appears in (3.5c) is not well defined; $\operatorname{curl}\mathbf{u} \notin L^2$ a priori. To understand the source of the difficulty—and how it is addressed—it helps to recall why $\mathbf{H}(\operatorname{div})$ enforces weak normal continuity, whereas $\mathbf{H}(\operatorname{curl})$ enforces weak tangential continuity.

$$\begin{array}{ccccccc} H^1_0 & \xrightarrow{\operatorname{grad}} & \mathbf{H}_0(\operatorname{curl}) & \xrightarrow{\operatorname{curl}} & \mathbf{H}_0(\operatorname{div}) & \xrightarrow{\operatorname{div}} & L^2_0 \\ \downarrow & & \downarrow & & \downarrow & & \downarrow \\ \mathbb{Q} & \xrightarrow{\operatorname{grad}} & \mathbb{V} & \xrightarrow{\operatorname{curl}} & \overline{\mathbb{V}} & \xrightarrow{\operatorname{div}} & \overline{\mathbb{Q}} \end{array} \tag{4.1}$$

Definition 4.1 (Mesh notation, jumps, averages, and penalty)**.** *We fix mesh and facet notations used throughout the interior–penalty construction (cf. [EG21a, Chap. 18]).*

i) Let $\mathcal{T}$ be a shape–regular mesh with cells $\mathcal{K}$ and facets $\mathcal{F}$. For each interior facet $F = \partial K_+ \cap \partial K_- \in \mathcal{F}$, let $\mathbf{n}_\pm$ denote the outward unit normals on $K_\pm$. In 2D, unit tangents $\mathbf{t}_\pm$ are obtained by rotating $\mathbf{n}_\pm$ clockwise by $\pi/2$.

ii) Local mesh sizes on either side of F are $h_\pm$ and the facet–averaged size is $h_F := \frac{1}{2}(h_+ + h_-)$.

iii) Let $\mathbf{u}_\pm$ denote the value of a discontinuous vector field on either side of F. We define the following jump operators: $[\![\mathbf{u}]\!]^* := \mathbf{u}_+ - \mathbf{u}_-$ and $[\![\mathbf{u} \times \mathbf{n}]\!] := \mathbf{u}_+ \times \mathbf{n}_+ + \mathbf{u}_- \times \mathbf{n}_-$. And let the arithmetic average across F be $\{\{\mathbf{u}\}\} := \frac{1}{2}(\mathbf{u}_+ + \mathbf{u}_-)$.

$\mathbf{H}$(div) and $\mathbf{H}$(curl) conformity

In $\mathbf{H}$(div) we only have L^2 bulk regularity, so pointwise traces need not exist. Elementwise Green's formula makes this precise: for any $\phi \in H^1(\Omega)$ and any mesh $\mathcal{T}$ with interior faces $\mathcal{F}_{\text{int}}$,

$$\begin{aligned}\sum_{\mathcal{K}\in\mathcal{T}} \int_{\mathcal{K}} \mathbf{u} \cdot \nabla\phi = &- \sum_{\mathcal{K}\in\mathcal{T}} \int_{\mathcal{K}} (\operatorname{div}\mathbf{u})\,\phi \\ &+ \sum_{F\in\mathcal{F}_{\text{int}}} \big\langle [\![\mathbf{u}\cdot\mathbf{n}]\!],\ \phi \big\rangle_F + \big\langle \gamma_n(\mathbf{u}),\ \phi \big\rangle_{\partial\Omega}.\end{aligned} \tag{4.2}$$

Here $[\![\mathbf{u} \cdot \mathbf{n}]\!] \in H^{-1/2}(F)$ is the normal–flux jump on $F = \partial\mathcal{K}_+ \cap \partial\mathcal{K}_-$. Thus, if the jump is nonzero, the divergence acts on test functions as

$$\langle \operatorname{div}\mathbf{u},\ \phi\rangle \ = \ \int_\Omega g\,\phi\,dx \ + \ \sum_F \int_F [\![\mathbf{u}\cdot\mathbf{n}]\!]\,\phi\,ds, \tag{4.3}$$

i.e. it contains a surface distribution $[\![\mathbf{u}\cdot\mathbf{n}]\!]\,\delta_F$ supported on F (a measure on the face), which is not an L^2 function. To keep $\operatorname{div}\mathbf{u} \in L^2$ (hence exact local conservation), we require *weak continuity* of the normal component: the two elementwise normal traces coincide in the trace space $H^{-1/2}(F)$,

$$\big\langle (\mathbf{u}|_{K_1}\cdot\mathbf{n}) - (\mathbf{u}|_{K_2}\cdot\mathbf{n}),\ \phi \big\rangle_F = 0 \qquad \forall\,\phi \in H^{1/2}(F). \tag{4.4}$$

Here $H^{-1/2}(F)$ is the dual of the boundary trace space $H^{1/2}(F)$ (the trace of H^1), so "weakly continuous" means "equal as functionals on $H^{1/2}(F)$," not pointwise. The normal–trace map $\gamma_n : \mathbf{H}(\operatorname{div}) \to H^{-1/2}(\partial\Omega)$ is bounded and weakly continuous, so this property is preserved under weak limits.

Everything above has a curl—twin: replace "normal flux" by *tangential trace* and "div" by curl. Concretely, to keep $\operatorname{curl}\mathbf{u} \in L^2$ one requires *weak tangential continuity* across each interior face F: the elementwise tangential traces coincide in the trace space,

$$\big\langle [\![\mathbf{n} \times \mathbf{u}]\!],\ \boldsymbol{\phi} \big\rangle_F = 0 \qquad \forall\,\boldsymbol{\phi} \in [H^{1/2}(F)]^d, \tag{4.5}$$

i.e. $\gamma_t(\mathbf{u}|_{\mathcal{K}_1}) = \gamma_t(\mathbf{u}|_{\mathcal{K}_2})$ in $[H^{-1/2}(F)]^d$. Otherwise $\operatorname{curl}\mathbf{u}$ acquires a *surface distribution* supported on F (the curl–analogue of the "surface charge" in $\mathbf{H}$(div)).

We now describe how the IPM enforces the missing $\mathbf{H}(\mathrm{curl})$ conformity.

Interior–penalty method (IPM)

In line with Ern & Guermond [EG21a, Ch. 18] [EG21b, Ch. 38], we define the broken $\mathbf{H}(\mathrm{curl})$ bilinear form on $\overline{\mathbb{V}}$

$$\begin{aligned}\mathcal{C}^*[\mathbf{u},\mathbf{v}] := \sum_{K\in\mathcal{K}}\int_K \operatorname{curl}\mathbf{u}\cdot\operatorname{curl}\mathbf{v} + \sum_{F\in\mathcal{F}}\int_F \Big[\frac{\sigma}{h_F}[\![\mathbf{u}]\!]^*\cdot[\![\mathbf{v}]\!]^* \\ - [\![\mathbf{u}\times\mathbf{n}]\!]\cdot\{\!\{\operatorname{curl}\mathbf{v}\}\!\} - \{\!\{\operatorname{curl}\mathbf{u}\}\!\}\cdot[\![\mathbf{v}\times\mathbf{n}]\!]\Big],\end{aligned} \tag{4.6}$$

where $\sigma > 0$ denotes the interior–penalty parameter. With $\mathcal{C}^*$ in hand, define the broken enstrophy

$$\mathcal{E}^*(\mathbf{u}) \;:=\; \mathcal{C}^*[\mathbf{u},\mathbf{u}] \;\geq 0, \tag{4.7}$$

and replace the ill–posed $(\operatorname{curl}\mathbf{u},\operatorname{curl}^2\boldsymbol{\chi})$ pairing by $\mathcal{C}^*[\mathbf{u},\operatorname{curl}\boldsymbol{\chi}]$; all other tests and terms remain as in (3.5). Hence, the IP semi–discrete formulation seeks $(\mathbf{u},p,\boldsymbol{\omega},\theta)\in\overline{\mathbb{V}}\times\overline{\mathbb{Q}}\times\mathbb{V}\times\mathbb{Q}$ such that

$$(\dot{\mathbf{u}},\mathbf{v}) = (\mathbf{u}\times\boldsymbol{\omega},\mathbf{v}) + (p,\operatorname{div}\mathbf{v}) - \frac{1}{\mathrm{Re}}(\operatorname{curl}\boldsymbol{\omega},\mathbf{v}), \tag{4.8a}$$

$$0 = (\operatorname{div}\mathbf{u},q), \tag{4.8b}$$

$$(\operatorname{curl}\boldsymbol{\omega},\operatorname{curl}\boldsymbol{\chi}) = \mathcal{C}^*[\mathbf{u},\operatorname{curl}\boldsymbol{\chi}] + (\nabla\theta,\boldsymbol{\chi}), \tag{4.8c}$$

$$0 = (\boldsymbol{\omega},\nabla\eta), \tag{4.8d}$$

for all $(\mathbf{v},q,\boldsymbol{\chi},\eta)\in\overline{\mathbb{V}}\times\overline{\mathbb{Q}}\times\mathbb{V}\times\mathbb{Q}$; with access only to (4.1).
The 2D analogoue of (4.6) defines a broken $\mathbf{H}(\mathrm{rot})$ bilinear form on $\overline{\mathbb{V}}$ with access to (3.36)

$$\begin{aligned}\mathcal{C}^*[\mathbf{u},\mathbf{v}] := \sum_{K\in\mathcal{K}}\int_K \operatorname{rot}\mathbf{u}\cdot\operatorname{rot}\mathbf{v}\,dx + \sum_{F\in\mathcal{F}}\int_F \Big[\frac{\sigma}{h_F}[\![\mathbf{u}]\!]^*\cdot[\![\mathbf{v}]\!]^* \\ - [\![\mathbf{u}\cdot\mathbf{t}]\!]\{\operatorname{rot}\mathbf{v}\} - \{\operatorname{rot}\mathbf{u}\}[\![\mathbf{v}\cdot\mathbf{t}]\!]\Big]ds.\end{aligned} \tag{4.9}$$

Accordingly, we replace the ill–defined $-(\operatorname{rot}\mathbf{u},\Delta\chi) = (\operatorname{rot}\mathbf{u},\operatorname{rot}(\operatorname{curl}\chi)$ pairing with $\mathcal{C}^*[\mathbf{u},\operatorname{curl}\chi]$. Therefore, find $(\mathbf{u},p,\omega)\in\overline{\mathbb{V}}\times\overline{\mathbb{Q}}\times\mathbb{U}$ such that

$$(\dot{\mathbf{u}},\mathbf{v}) = (\omega\,\mathbf{u}_\perp,\mathbf{v}) + (p,\operatorname{div}\mathbf{v}) - \frac{1}{\mathrm{Re}}(\operatorname{curl}\omega,\mathbf{v}), \tag{4.10a}$$

$$0 = (\operatorname{div}\mathbf{u},q), \tag{4.10b}$$

$$(\nabla\omega,\nabla\chi) = \mathcal{C}^*[\mathbf{u},\operatorname{curl}\chi], \tag{4.10c}$$

for all $(\mathbf{v},q,\chi)\in\overline{\mathbb{V}}\times\overline{\mathbb{Q}}\times\mathbb{U}$.

Remark 4.2 (Penalty tuning in practice)**.** *The facet penalty σ penalises interelement tangential trace jumps, thereby weakly enforcing the continuity that full $H(\mathrm{curl})$ conformity would impose. In the formal limit $\sigma \to \infty$ these jumps are driven to zero, although the discrete space itself remains broken. Numerically, σ must be finite: on shape–regular meshes we use the standard scaling $\sigma \simeq c\,p^2/h$ (with local polynomial degree p and facet size h), which secures coercivity of the broken bilinear form for moderate c while avoiding the ill–conditioning caused by overly large penalties.*

4.3 Conforming Workaround

To motivate our conforming approach, we begin by introducing the key ideas of the reparametrisation framework from Ainsworth & Parker [AP24a; AP24b].

Biharmonic without C^1 elements

Let $\Omega \subset \mathbb{R}^2$ be a simply connected Lipschitz domain. The weak formulation of the biharmonic BVP reads:

$$\text{Find } u \in H^2_0(\Omega): \qquad (\Delta u, \Delta v) = (f, v) \quad \forall v \in H^2_0(\Omega). \tag{4.11}$$

Standard Galerkin discretisations require H^2–conforming (C^1) FEs. In line with [AP24a; AP24b], we exploit the exact–sequence isomorphism[a]

$$\operatorname{grad} : H^2_0(\Omega) \;\cong\; \{\mathbf{g} \in H^1(\Omega;\mathbb{R}^2) : \operatorname{rot}\mathbf{g} = 0\} \tag{4.12}$$

so that the biharmonic weak form (4.11) can be recast in H^1–conforming spaces via a FEEC–based mixed formulation (4.14). The procedure is:

Step 1: Pre–processing (Poisson solve): Find $z \in \mathbb{CG}$[b] such that

$$(\nabla z, \nabla v) = (f, v) \quad \forall v \in \mathbb{CG}. \tag{4.13}$$

Step 2: Mixed formulation: Find $(\mathbf{g}, r) \in [\mathbb{CG}]^2 \times \mathbb{CG}$ such that

$$\begin{aligned} (\nabla\mathbf{g}, \nabla\boldsymbol{\psi}) + (\operatorname{rot}\boldsymbol{\psi}, r) &= (\nabla z, \nabla\boldsymbol{\psi}) \quad \forall \boldsymbol{\psi} \in [\mathbb{CG}]^2, \\ (\operatorname{rot}\mathbf{g}, s) &= 0^{[1]} \qquad\quad \forall s \in \mathbb{CG}. \end{aligned} \tag{4.14}$$

[c]

Step 3: Post–processing: Find $u \in \mathbb{CG}$ such that

$$(\nabla u, \nabla v) = (\mathbf{g}, \nabla v) \quad \forall v \in \mathbb{CG}. \tag{4.15}$$

Uniqueness of u follows from Poincaré's inequality on $H^1_0(\Omega)$. Furthermore, since $\mathbf{g} \in \operatorname{grad}(\mathbb{HCT})$, the recovered scalar field u coincides with the H^2-conforming Galerkin solution in $\mathbb{HCT}$ of (4.11), see Lemma 3.1 of [AP24a].

[a]Where $\operatorname{rot}\mathbf{g} := \partial_x g_2 - \partial_y g_1$ in 2D.
[b]Continuous Galerkin (CG, a.k.a. Lagrange)
[c]This enforces $\operatorname{rot}\mathbf{g} = 0$, i.e. $\mathbf{g}$ lies in the discrete gradient subspace.

This three–step procedure eliminates the need for C^1 basis functions, replacing them by two second–order Poisson solves and one Stokes–type saddle–point problem, all posed in H^1–conforming FE spaces. This methodology relies on the *exactness* of the Stokes complex (2.17b), where $\mathcal{N}(\mathrm{rot}) = \mathcal{R}(\mathrm{grad})$ in $\mathbf{H}^1(\Omega;\mathbb{R}^2)$ ensures that solutions $\mathbf{g}$ of Step 2 lie in $\mathrm{grad}(H_0^2(\Omega))$.

Motivated by the above *eliminate excessive regularity via exact sequences* idea, we now treat the velocity–vorticity Navier–Stokes discretisation (3.5)–(3.7). In 3D, we introduce an auxiliary field $\boldsymbol{\alpha}$ and enforce $\boldsymbol{\alpha} = \operatorname{curl}\boldsymbol{\omega}$ variationally in (3.5). Find $((\mathbf{u},\boldsymbol{\alpha}),(p,r),\boldsymbol{\omega},\theta) \in \overline{\mathbb{V}}^2 \times \overline{\mathbb{Q}}^2 \times \hat{\mathbb{V}} \times \hat{\mathbb{Q}}$ such that[2]

$$(\dot{\mathbf{u}},\mathbf{v}) = (\mathbf{u}\times\boldsymbol{\omega},\mathbf{v}) + (p,\operatorname{div}\mathbf{v}) - \frac{1}{\mathrm{Re}}(\boldsymbol{\alpha},\mathbf{v}), \tag{4.16a}$$

$$0 = (\operatorname{div}\mathbf{u},q), \tag{4.16b}$$

$$(\boldsymbol{\alpha},\boldsymbol{\beta}) = (\operatorname{curl}\mathbf{u},\operatorname{curl}\boldsymbol{\beta}) + (r,\operatorname{div}\boldsymbol{\beta}), \tag{4.16c}$$

$$0 = (\operatorname{div}\boldsymbol{\alpha},s), \tag{4.16d}$$

$$(\operatorname{curl}\boldsymbol{\omega},\operatorname{curl}\boldsymbol{\chi}) = (\boldsymbol{\alpha},\operatorname{curl}\boldsymbol{\chi}) - (\nabla\theta,\boldsymbol{\chi}), \tag{4.16e}$$

$$0 = -(\boldsymbol{\omega},\nabla\eta) \tag{4.16f}$$

for all $((\mathbf{v},\boldsymbol{\beta}),(q,s),\boldsymbol{\chi},\eta) \in \overline{\mathbb{V}}^2 \times \overline{\mathbb{Q}}^2 \times \hat{\mathbb{V}} \times \hat{\mathbb{Q}}$[3]. Here, the FE spaces induce a discrete de Rham complex of standard reduced regularity[4]. This is equivalent to solving (3.5) over the discrete Stokes complex

$$\begin{array}{ccccccc} H_0^1 & \xrightarrow{\text{grad}} & \mathbf{H}(\operatorname{grad}\operatorname{curl}) \cap \mathbf{H}_0(\operatorname{curl}) & \xrightarrow{\text{curl}} & \mathbf{H}^1 \cap \mathbf{H}_0(\operatorname{div}) & \xrightarrow{\text{div}} & L_0^2 \\ \downarrow & & \downarrow & & \downarrow & & \downarrow \\ \hat{\mathbb{Q}} & \xrightarrow{\text{grad}} & \operatorname{grad}\hat{\mathbb{Q}} \oplus \operatorname{curl}^{-1}\overline{\mathbb{U}} & \xrightarrow{\text{curl}} & \overline{\mathbb{V}} & \xrightarrow{\text{div}} & \overline{\mathbb{Q}} \end{array} \tag{4.17}$$

[2]We represent viscosity by a curl–curl L^2–Riesz map for a divergence-free surrogate $\boldsymbol{\alpha}$ and use exactness to identify $\boldsymbol{\alpha}$ with $\operatorname{curl}\boldsymbol{\omega}$ (cf. (4.14)). Concretely, find $(\boldsymbol{\alpha},r) \in \mathbf{H}_0(\operatorname{div}) \times \overline{\mathbb{Q}}$ such that $(\boldsymbol{\alpha},\boldsymbol{\beta}) + (r,\operatorname{div}\boldsymbol{\beta}) = (\operatorname{curl}\mathbf{u},\operatorname{curl}\boldsymbol{\beta})$ for all $\boldsymbol{\beta} \in \overline{\mathbb{V}}$ and $(\operatorname{div}\boldsymbol{\alpha},s) = 0$ for all $s \in \overline{\mathbb{Q}}$; together with the coupling $(\operatorname{curl}\boldsymbol{\omega},\operatorname{curl}\boldsymbol{\chi}) = (\boldsymbol{\alpha},\operatorname{curl}\boldsymbol{\chi}) - (\nabla\theta,\boldsymbol{\chi})$ for all $\boldsymbol{\chi} \in \hat{\mathbb{V}}$, exactness $\ker(\operatorname{div}|_{\overline{\mathbb{V}}}) = \operatorname{curl}(\overline{\mathbb{U}})$ yields $\boldsymbol{\alpha} = \operatorname{curl}\boldsymbol{\omega}$.

[3]The strong form of (4.16) recovers the NS equations exactly, with $\boldsymbol{\alpha} = \operatorname{curl}^2\mathbf{u}$ and $\boldsymbol{\omega} = \operatorname{curl}\mathbf{u}$ for an exact solution.

[4]Where $\hat{\mathbb{Q}} \in H_0^1$, $\hat{\mathbb{V}} \in \mathbf{H}_0(\operatorname{curl})$, $\overline{\mathbb{V}} \in \mathbf{H}_0(\operatorname{div})$ and $\overline{\mathbb{Q}} \in L_0^2$.

where $\operatorname{curl}^{-1}\overline{\mathbb{U}}$ maps to the discrete divergence–free space $\hat{\mathbb{U}}$. Similar to the argument in §3.3, energy stability follows by testing (4.16) with $(\mathbf{v},\boldsymbol{\beta},q)=(\mathbf{u},\mathbf{u},p-\frac{1}{\mathrm{Re}},r)$; whereas enstrophy follows by testing (4.16) with $(\mathbf{v},\boldsymbol{\beta},s)=(\boldsymbol{\alpha},\dot{\mathbf{u}},p)$. Lastly, Equation 4.16, in 2D, reduces to the following semidiscretisation: find $((\mathbf{u},\boldsymbol{\alpha}),(p,r),\omega)\in\overline{\mathbb{V}}^2\times\overline{\mathbb{Q}}^2\times\hat{\mathbb{U}}$ such that

$$(\dot{\mathbf{u}},\mathbf{v}) = (\omega\mathbf{u}_\perp,\mathbf{v}) + (p,\operatorname{div}\mathbf{v}) - \frac{1}{\mathrm{Re}}(\boldsymbol{\alpha},\mathbf{v}), \tag{4.18a}$$

$$0 = (\operatorname{div}\mathbf{u},q), \tag{4.18b}$$

$$(\boldsymbol{\alpha},\boldsymbol{\beta}) = (\operatorname{rot}\mathbf{u},\operatorname{rot}\boldsymbol{\beta}) + (r,\operatorname{div}\boldsymbol{\beta}), \tag{4.18c}$$

$$0 = (\operatorname{div}\boldsymbol{\alpha},s), \tag{4.18d}$$

$$(\operatorname{curl}\omega,\operatorname{curl}\chi) = (\boldsymbol{\alpha},\operatorname{curl}\chi) \tag{4.18e}$$

for all $((\mathbf{v},\boldsymbol{\beta}),(q,s),\chi)\in\overline{\mathbb{V}}^2\times\overline{\mathbb{Q}}^2\times\hat{\mathbb{U}}$. Here, the FE spaces induce a two–dimensional discrete de Rham complex[5]. This again is equivalent to solving (3.7) over the following Stokes complex

$$\begin{array}{ccccc} H^2\cap H_0^1 & \xrightarrow{\operatorname{curl}} & \mathbf{H}^1\cap\mathbf{H}_0(\operatorname{div}) & \xrightarrow{\operatorname{div}} & L_0^2 \\ \downarrow & & \downarrow & & \downarrow \\ \operatorname{curl}^{-1}\overline{\mathbb{U}} & \xrightarrow{\operatorname{curl}} & \overline{\mathbb{V}} & \xrightarrow{\operatorname{div}} & \overline{\mathbb{Q}} \end{array} \tag{4.19}$$

In 2D, to derive energy and enstrophy stability, test (4.18) against $(\mathbf{v},\boldsymbol{\beta})=(\mathbf{u},\mathbf{u})$ and $(\mathbf{v},\boldsymbol{\beta})=(\boldsymbol{\alpha},\dot{\mathbf{u}})$, respectively.

[5]Where $\hat{\mathbb{U}}\in H_0^1$, $\overline{\mathbb{V}}\in\mathbf{H}_0(\operatorname{div})$ and $\overline{\mathbb{Q}}\in L_0^2$ (cf. (3.36)).

"Beware of bugs in the above code; I have only proved it correct, not tried it."

— Donald E. Knuth

5 Numerical experiments

Contents

The apparatus is ready: a conforming Stokes–complex discretisation (4.16)–(4.18), and a non–conforming interior–penalty counterpart (4.8)–(4.10). We now turn our attention to certain numerical experiments in this chapter. These probe whether preserving the continuous algebra at the discrete level translates into any robust behaviour on under–resolved meshes.

5.1 2D shear test

The principal benefit of enstrophy–stable schemes—namely, an Re–independent bound on $\|\nabla \mathbf{u}\|$ (cf. Lemma 3.8)—is best demonstrated in flows that excite shear–driven instabilities. The shear layer test, commonly used in SP literature [PG17; Zha+24], thus serves as a comprehensive test for long–time stability. As the initial perturbation amplifies and vortices interact, any imbalance in discrete energy or enstrophy compounds and exposes drift or blow–up. In the Euler limit $\mathrm{Re} = \infty$, a

structure–preserving scheme should conserve the relevant invariants while allowing physically meaningful instabilities to evolve without artificial damping or numerical energy growth. Under–resolved simulations often highlight the difference: non–mimetic methods may exhibit numerical instabilities, while structure–preserving schemes are designed to suppress such artefacts. We therefore include the shear layer test to assess whether our discretisation accurately captures the nonlinear dynamics over long times while preserving the expected behaviour of energy and enstrophy. To exercise these properties, we next choose a conforming initial condition on $\Omega = (0,1)^2$:

$$\psi_0(x,y) = \delta\left[\operatorname{lncosh}\left(\tfrac{1}{2\delta}\right) - \operatorname{lncosh}\left(\tfrac{y-\frac{1}{2}}{\delta}\right)\right] - A\cos(2\pi x)\sin(2\pi y), \tag{5.1}$$

such that $\psi_0 \in H^1(\Omega)$, $\mathbf{u}_0 = \operatorname{rot}\psi_0 \in \mathbf{H}(\operatorname{div})$, and $\omega_0 = \operatorname{rot}\mathbf{u}_0 \in L^2(\Omega)$. Choosing $\delta = \mathcal{O}(h)$ resolves the interface at mesh scale and $A \ll 1$ seeds Kelvin–Helmholtz roll–up; by construction $\psi_0|_{y=0,1} = 0$ and $\sin(2\pi y) = 0$ on $y = 0, 1$, so the y–Dirichlet and x–periodic constraints hold exactly at $t = 0$. This IC (5.1) contains a sharp velocity gradient (a smoothed step function), so discretisation errors in representing this gradient immediately show up as vorticity errors. At the shear interface, a poorly constructed method might result in inaccurate vorticity or Gibbs oscillations. Such errors can feed back into the momentum equation, leading to unphysical energy gain or loss of enstrophy; structure–preserving methods are designed to mitigate this. Assuming the mesh to be quadrilateral, let $\mathbb{CG}_{p+2}$ and $\mathbb{DG}_p$ denote the continuous and discontinuous Galerkin spaces of degree $p+2$ and p, respectively (see [EG21a]). The Brezzi–Douglas–Marini space $\mathbb{BDM}_p$ [BDM85] is defined as

$$\mathbb{BDM}_p := [\mathbb{DG}_p]^2 \cap \mathbf{H}(\operatorname{div}), \tag{5.2}$$

we note that, for $p \geq 0$, this induces a discrete de Rham complex

$$\mathbb{CG}_{p+2} \xrightarrow{\text{curl}} \mathbb{BDM}^{\mathrm{d}}_{p+1} \xrightarrow{\text{div}} \mathbb{DG}_p. \tag{5.3}$$

This complex (5.3) is non–conforming ($\mathbb{BDM}_p \not\subset \mathbf{H}(\operatorname{curl})$), thus necessitating the use of our non–conforming IP scheme (4.10). We compare 3 different one–stage integrators: a classical energy–stable scheme[1], the comparable MEEVC scheme

[1]The classical energy–stable discretisation: find $(\mathbf{u}, p) \in \overline{\mathbb{V}} \times \overline{\mathbb{Q}}$ such that

$$(\dot{\mathbf{u}}, \mathbf{v}) = \sum_{K\in\mathcal{K}} \int_K (\operatorname{rot}\mathbf{u})\,\mathbf{k}\cdot(\mathbf{u}\times\mathbf{v}) - \sum_{F\in\mathcal{F}} \int_F [\![\mathbf{u}\cdot\mathbf{t}]\!]\,\mathbf{k}\cdot(\{\{\mathbf{u}\}\}\times\{\{\mathbf{v}\}\}) + (p, \operatorname{div}\mathbf{v}), \tag{5.4a}$$

$$0 = (\operatorname{div}\mathbf{u}, q), \tag{5.4b}$$

for all $(\mathbf{v}, q) \in \overline{\mathbb{V}} \times \overline{\mathbb{Q}}$.

of Palha & Gerritsma [PG17], and our non–conforming discretisation (4.10) with $\sigma = 2^5$ and timestep $\Delta t = 2^{-8}$. Figure 5.1 shows plots of the stream function ψ at three different times $t = \{0, 2^0, 2^2\}$. At $\mathrm{Re} = \infty$, the three discretisations exhibit different visible onset times of Kelvin–Helmholtz activity. In the classical baseline, small billows appear along the interface at about $t \approx 2^0 - 2^{-3}$. In the MEEVC run, comparable features emerge slightly later, at about $t \approx 2^0 + 2^{-2}$. In our IPM run, no clear roll–up is seen within the time window $t \in [0, 2^2]$; the layer remains essentially one–dimensional, with only a very slight deformation discernible near $t \approx 2^2$.

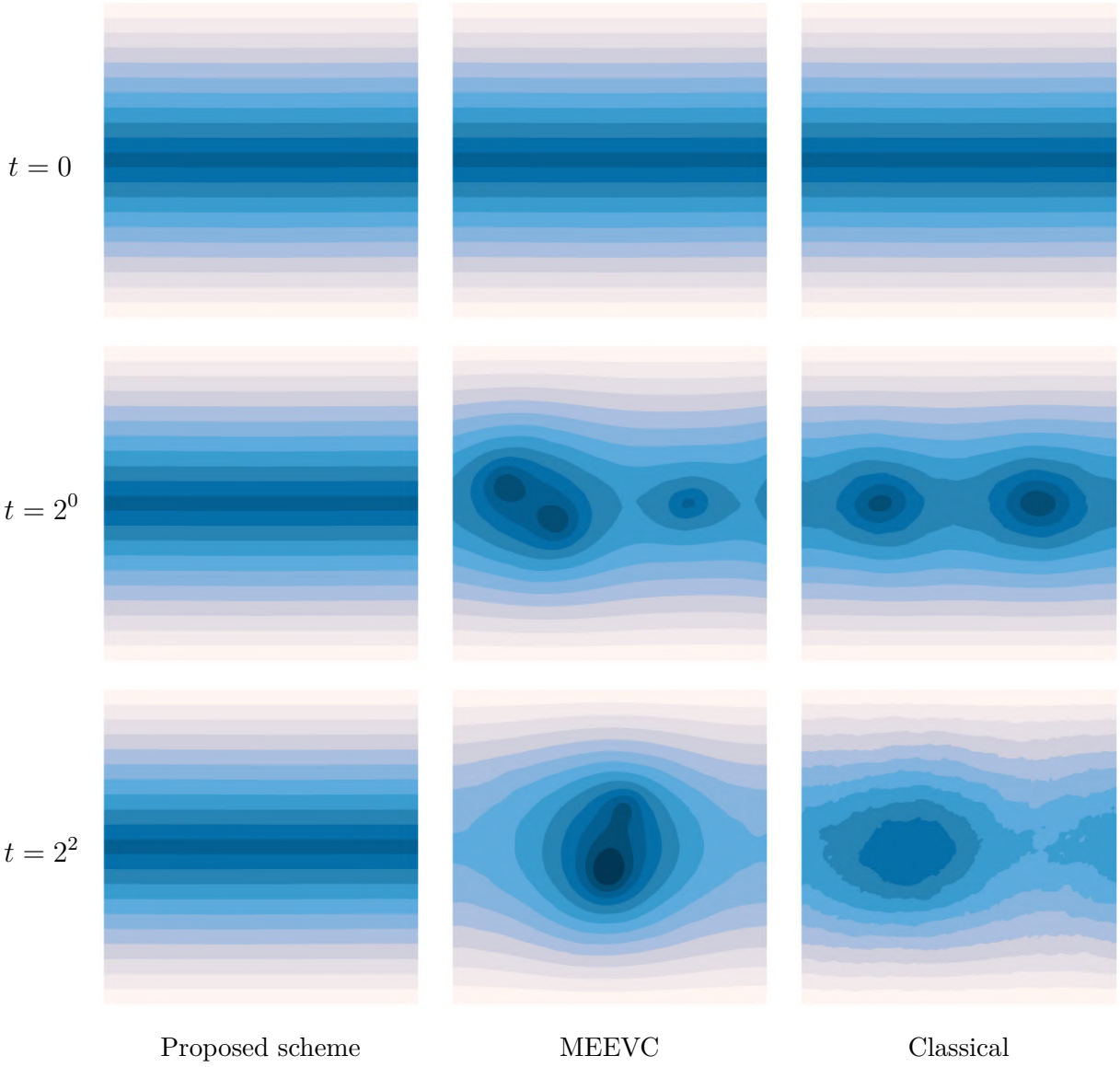

Figure 5.1: Comparison of the shear layer across 4 time steps (rows) and three methods (columns): Proposed scheme, MEEVC, and Classical.

Since we are comparing non–conforming discretisations, there are various notions

of enstrophy available: the broken enstrophy $\mathcal{E}^*(\mathbf{u}) = \mathcal{C}^*[\mathbf{u},\mathbf{u}]$ is the interior–penalty (nonconforming) H^2–energy of (4.10) and therefore includes facet penalty contributions in addition to cell–interior terms; the internal enstrophy $\hat{\mathcal{E}}(\mathbf{u}) = \frac{1}{2}\sum_{K\in\mathcal{K}} \|\operatorname{rot}\mathbf{u}\|^2$ is the purely cell–interior L^2–energy of $\operatorname{rot}\mathbf{u}$; and the auxiliary enstrophy $\tilde{\mathcal{E}} = \frac{1}{2}\|\omega\|^2$ refers to the L^2–energy of the auxiliary vorticity ω preserved by MEEVC–type formulations.

Figure 5.2a reports the broken (solid lines) and internal (dashed lines) enstrophy of the primal velocity. Our proposed integrator remains essentially flat at its initial level in both measures over the full time window. The MEEVC run exhibits a short start–up rise (coincident with the first visible Kelvin–Helmholtz activity) and thereafter oscillates about a plateau in both curves. The classical baseline shows a sharp early spike, quickly reaching a very large amplitude $6 \cdot 10^5$. Figure 5.2b illustrates the evolution of the auxiliary enstrophy: both MEEVC and our method maintain this quantity at a constant level—a result to be expected, since MEEVC enforces the auxiliary variable to be preserved.

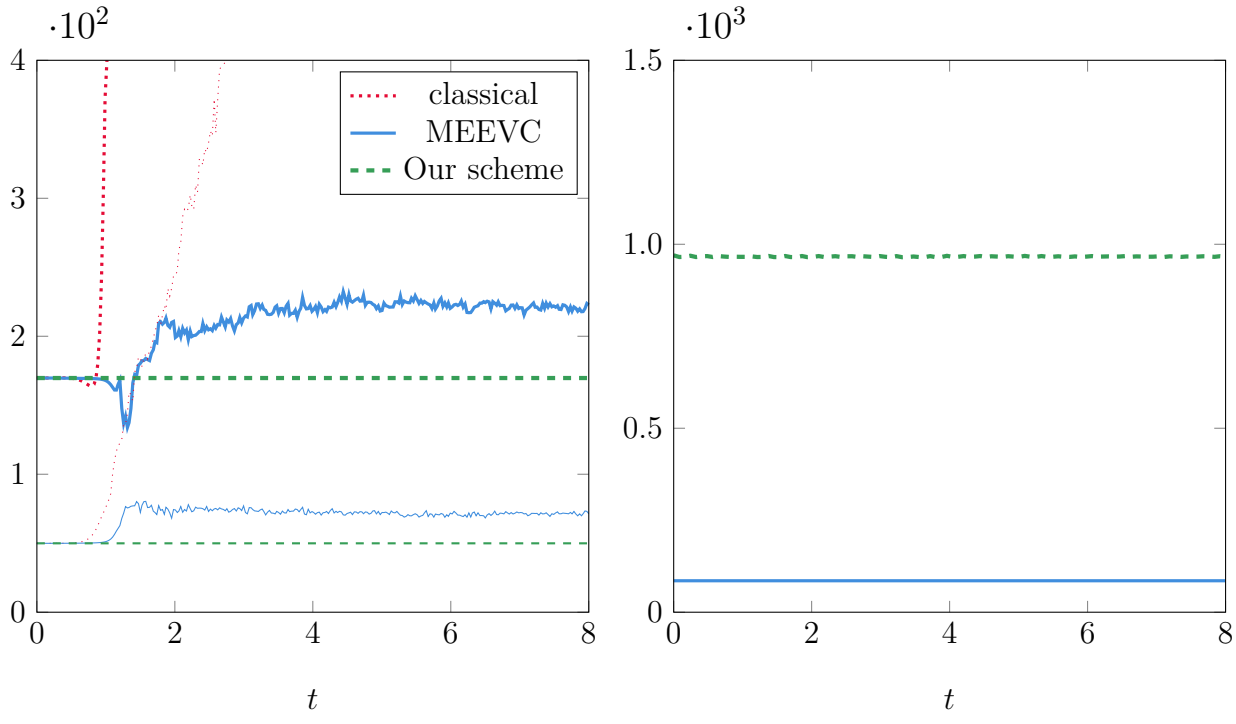

(a) Broken and internal enstrophy

(b) Auxiliary enstrophy

Figure 5.2: Evolution in different forms of the enstrophy for 3 different 1–stage integrators in the 2D vortex test. In Figure 5.2a the broken $\mathcal{E}^*$ is plotted with *thick* lines (upper curves), while and internal enstrophies is plotted with *thin, dashed* lines (lower curves); Figure 5.2b shows the auxiliary enstrophy $\tilde{\mathcal{E}}(\omega) = \frac{1}{2}\|\omega\|^2$. The legend is shown only in (a).

5.2 2D vortex test

Next, to further demonstrate the structure–preserving properties (see §3.3) of our scheme, we look at the evolution of a counter–rotating vortex dipole in a 2D unit box $\Omega = (0,1)^2$ at the inviscid limit $\mathrm{Re} = \infty$. Similar vortex and Taylor–Green tests are commonly employed to validate structure–preserving discretisations [PG17; Zha+24]. To set up the initial condition, we define the Weierstrass elliptic function $\wp(z) : \mathbb{C} \to \mathbb{C}$ on the square lattice $2\mathbb{Z} + 2i\mathbb{Z}$ as

$$\wp(z) := \frac{1}{z^2} + \sum_{\substack{(m,n)\in \\ \mathbb{Z}^2\setminus\{(0,0)\}}} \frac{1}{(z-2m-2ni)^2} - \frac{1}{(2m+2ni)^2}, \tag{5.5}$$

truncated to $|m|, |n| \leq N$, with $N = 2^3$ in the following runs. Equation 5.5 is a meromorphic[2] and doubly periodic function. We fix two distinct centers $z_\pm = x_\pm + iy_\pm$ and define the stream function

$$\begin{aligned} \psi_0(x,y) \;\propto\; & \Re\Big\{ \log\left[\wp(z) - \wp(z_+)\right] - \log\left[\wp(z) - \wp(\overline{z_+})\right] \Big\} \\ & - \Re\Big\{ \log\left[\wp(z) - \wp(z_-)\right] - \log\left[\wp(z) - \wp(\overline{z_-})\right] \Big\}, \end{aligned} \tag{5.6}$$

where $\overline{*}$ denotes the complex conjugate of $*$, and $\Re : \mathbb{C} \to \mathbb{R}$ is the real component. The first bracket places a single vortex at z_+ (with an image at $\overline{z_+}$), and the second places an oppositely signed vortex at z_-; the difference realises a counter–rotating dipole. In our runs we set $(x_+, y_+) = \left(\frac{2}{\varphi} - 1, \frac{2}{\varphi^2}\right)$ and $(x_-, y_-) = \left(\frac{2}{\varphi^2}, \frac{2}{\varphi} - 1\right)$, with $\varphi = \frac{1+\sqrt{5}}{2}$. Since $\log \circ \wp$ is analytic away from the marked points, ψ_0 is harmonic on $\Omega \setminus \{z_+, z_-\}$, hence $-\Delta\psi_0 = 0$ (equivalent to (2.14)) on $\partial\Omega$. Moreover, by the square–lattice symmetries of $\wp$, the streamlines are tangent to $\partial\Omega$, so the induced velocity $\mathbf{u} = \operatorname{curl}\psi_0$ satisfies the no–flux condition $\mathbf{u}\cdot\mathbf{n} = 0$ on the boundary. These ICs (5.5) do not have a well–defined enstrophy, i.e. $\mathbf{u}_0$ is not $\mathbf{H}(\mathrm{curl})$–conforming. This ceases to be an issue up to projection onto $\overline{\mathbb{V}} \times \overline{\mathbb{Q}}$: find $(\mathbf{u}_0, p_0) \in \overline{\mathbb{V}} \times \overline{\mathbb{Q}}$ such that,

$$(\mathbf{u}_0, \mathbf{v}) = (p_0, \operatorname{div}\mathbf{v}) - (\psi_0, \operatorname{rot}\mathbf{v}), \tag{5.7a}$$

$$0 = (\operatorname{div}\mathbf{u}_0, q), \tag{5.7b}$$

for all $(\mathbf{v}, q) \in \overline{\mathbb{V}} \times \overline{\mathbb{Q}}$. We scale $\mathbf{u}_0 \leftarrow \mathbf{u}_0 / \sqrt{\frac{1}{2}\|\mathbf{u}_0\|^2}$ to normalize the energy. With $\mathbf{u}_0$ fixed, we now integrate (4.18) on $\Omega = (0,1)^2$ discretised by an Alfeld–split triangular mesh, employing the implicit midpoint time step.

[2] *Meromorphic* means holomorphic on $\mathbb{C} \setminus \Lambda$ with at most isolated poles on Λ (no essential singularities). For the Weierstrass $\wp$ associated with the lattice $\Lambda = 2\mathbb{Z} + 2i\mathbb{Z}$, the poles are exactly at the lattice points, each of order 2.

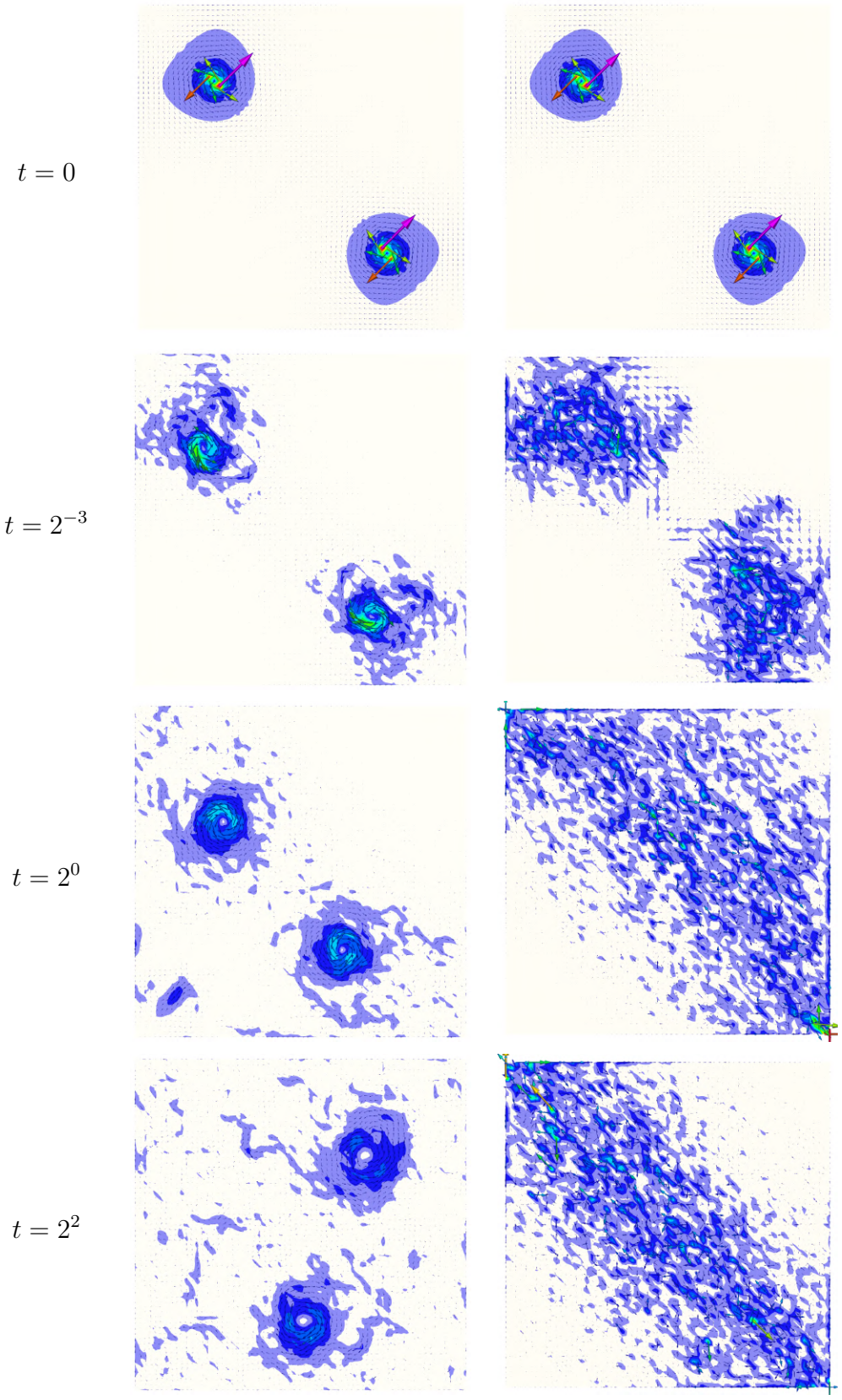

Figure 5.3: Contour plots of the velocity field $\mathbf{u}$ using two different one–stage integrators, shown at times $t = \{0, 2^{-3}, 2^{0}, 2^{2}\}$. The color scale ranges from red at $\|\mathbf{u}\| = 20$ to white at $\|\mathbf{u}\| = 0$. For simulation videos, see [Sha25]; for additional snapshots, see Appendix A.

The FE spaces $\mathbb{CG}_{p+2}$, $\mathbb{CG}_{p+1}$, and $\mathbb{DG}_p$ are continuous and discontinous Galerkin spaces of degree $p+2$, $p+1$, and p respectively. For $p \geq 0$, this induces a discrete Stokes complex

$$\mathbb{CG}_{p+2} \xrightarrow{\text{curl}} [\mathbb{CG}_{p+1}]^2 \xrightarrow{\text{div}} \mathbb{DG}_p. \tag{5.8}$$

For these FE spaces, $\text{curl}^{-1}\mathbb{U} \subset H^2 \cap H^1_0$ in (4.19) is the Morgan–Scott space $\mathbb{MS}$ [MS75]. For comparison, we run the energy– and enstrophy–stable integrator (4.18) alongside a classical energy–stable baseline, both at $\text{Re} = \infty$; deliberately under–resolved (so any spurious oscillation is immediately visible). Figure 5.3 shows snapshots of $\mathbf{u}$ at $t \in \{0, 2^{-3}, 2^0, 2^2\}$. In the structure–preserving run the two vortices remain compact and nearly axisymmetric throughout, with only weak spiral arms of vorticity and no discernible grid–scale artefacts. By contrast, the classical baseline shows small–scale noise and loss of coherence already at $t = 2^{-3}$; by $t = 2^0 - 2^2$ the vorticity field exhibits pronounced filamentation and directional smearing. Taken together, these observations indicate that, on under–resolved meshes, strict enforcement of energy and enstrophy suppresses aliasing–driven spurious enstrophy production without ad hoc damping, thereby preserving coherent vortical structures over long time integrations.

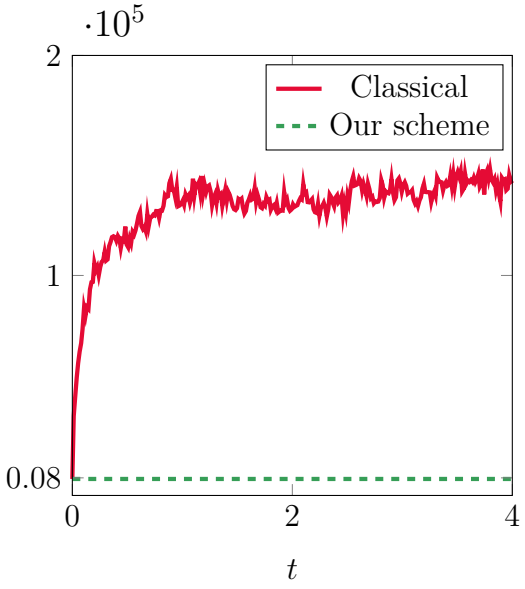

Figure 5.4: Evolution of enstrophy in the 2D vortex test Figure 5.3.

Figure 5.4 shows the evolution of enstrophy within each of the simulations, up to time $t = 2^2$; we need not plot the energies for each simulation, as each scheme is energy–stable. The classical, energy–only discretisation exhibits rapid enstrophy growth

and spurious fine–scale oscillations (see Figure 5.3) associated with the loss of a meaningful $\mathbf{H}^1$ bound (see §1.1.2) on coarse meshes, whereas the proposed structure–preserving scheme maintains enstrophy and therefore avoids these artifacts.

5.3 3D vortex test

The role of enstrophy evolution in 3D remains uncertain, particularly since enstrophy ceases to be a conserved quantity. As discussed in §1.1.3, it is still unclear whether preserving its evolution numerically—via (3.28)—has any bearing on the qualitative behaviour of solutions. To examine this, we conduct a numerical test to assess whether such preservation offers any tangible benefit. We consider a stationary Hill spherical vortex [Hil94] with swirling motion [Mof69, Sec.6]. In spherical coordinates (r, θ, φ), we define the Stokes stream function as

$$\psi(r,\theta,\varphi) := \begin{cases} 2\left[\dfrac{J_{3/2}(4\eta r)}{(4r)^{3/2}} - J_{3/2}(\eta)\right](r\sin\theta)^2, & r \le \frac{1}{4}, \\ 0, & r > \frac{1}{4}, \end{cases} \tag{5.9}$$

where J_ν denotes the Bessel function of the first kind of order ν and $\eta \approx 5.76$ is the first positive zero of $J_{5/2}$. Up to projection, the initial velocity is the Hill field

$$\mathbf{u}_{\text{raw}} = \frac{\partial_\theta \psi}{r^2 \sin\theta}\,\hat{\mathbf{r}} - \frac{\partial_r \psi}{r\sin\theta}\,\hat{\boldsymbol{\theta}} + \frac{4\eta\,\psi}{r\sin\theta}\,\hat{\boldsymbol{\varphi}}, \qquad (r \le \frac{1}{4}), \tag{5.10}$$

where $(\hat{\mathbf{r}}, \hat{\boldsymbol{\theta}}, \hat{\boldsymbol{\varphi}})$ denote the spherical unit vectors, and ∂_θ, ∂_r are partial derivatives with respect to θ and r, respectively. We form the discrete no–slip, divergence–free initial condition by the Leray projection [GR12]: find $(\mathbf{u}_0, p_0) \in \overline{\mathbb{V}} \times \overline{\mathbb{Q}}$ such that

$$(\mathbf{u}_0, \mathbf{v}) \;-\; (p_0, \operatorname{div}\mathbf{v}) = (\mathbf{u}_{\text{raw}}, \mathbf{v}), \tag{5.11a}$$

$$(\operatorname{div}\mathbf{u}_0, q) = 0. \tag{5.11b}$$

for all $(\mathbf{v}, q) \in \overline{\mathbb{V}} \times \overline{\mathbb{Q}}$. Then set $\mathbf{u}_0 \leftarrow \mathbf{u}_0 / \sqrt{\frac{1}{2}\|\mathbf{u}_0\|^2}$. With $\mathbf{u}_0$ fixed by (5.11), we now integrate the conforming workaround (4.16) on $\Omega = (0,1)^3$, with an Alfeld–split tetrahedral mesh. We employ the Scott–Vogelius pair for velocity–pressure (see Ern & Guermond [EG21a, Sec. 6 & 7]) and curl–conforming Nédélec element of the second kind [Néd86] for the auxiliary fields:

$$\widehat{\mathbb{Q}} = \mathbb{CG}_{p+3}, \qquad \widehat{\mathbb{V}} = \mathbb{N}\mathrm{ed}^{\mathrm{curl}}_{p+2}, \qquad \overline{\mathbb{V}} = [\mathbb{CG}_{p+1}]^3, \qquad \overline{\mathbb{Q}} = \mathbb{DG}_p. \tag{5.12}$$

These choices realise the discrete stokes complex (cf. (2.9))

$$\mathbb{CG}_{p+2} \xrightarrow{\text{grad}} \mathbb{N}\mathrm{ed}^{\mathrm{curl}}_{p+2} \xrightarrow{\text{curl}} [\mathbb{CG}_{p+1}]^3 \xrightarrow{\text{div}} \mathbb{DG}_p. \tag{5.13}$$

We fix the degree $p = 3$; this ensures $\operatorname{div} \overline{\mathbb{V}} = \overline{\mathbb{Q}}$ and inf–sup stability [FMS24]. For comparison, we run simulations using our three–dimensional conforming scheme (4.16) alongside a classical one that is solely energy–stable, with timestep $\Delta t = 2^{-10}$, and Reynolds number $\mathrm{Re} = 2^{16}$. Figure 5.5 displays cross–sections of streamlines of the velocity $\mathbf{u}$ at selected times, illustrating the evolution of the Hill vortex under both discretisations.

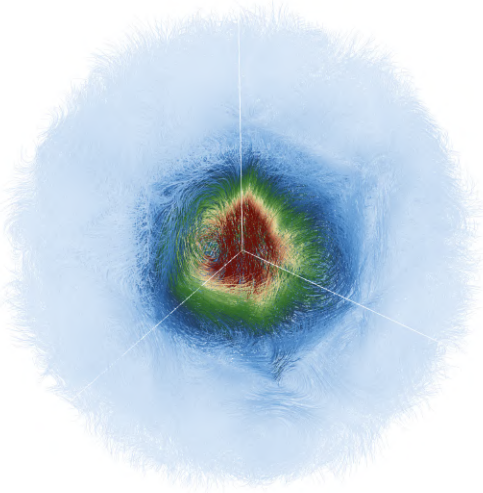

(a) $t = 0$

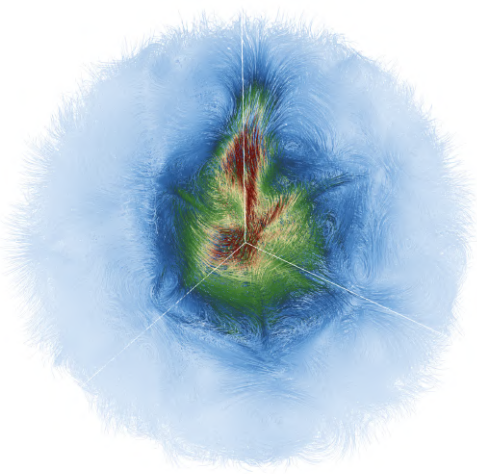

(b) $(\mathcal{K}, \mathcal{E})$–preserving; $t = 2^{-5}$

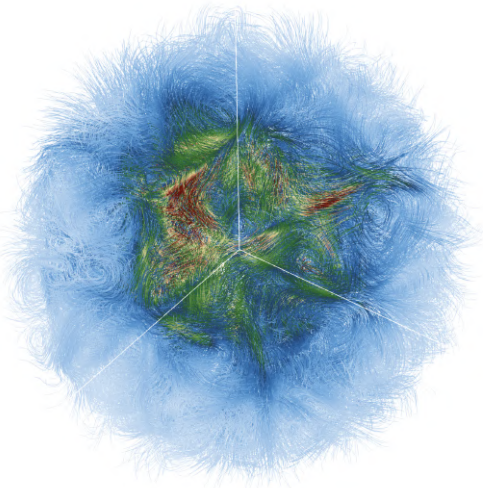

(c) $\mathcal{K}$–preserving; $t = 2^{-5}$

Figure 5.5: Cross sections of streamlines of the velocity field $\mathbf{u}$ for the Hill vortex at times $t \in \{0, 2^{-5}\}$ with $\mathrm{Re} = 2^{16}$ and $\Delta t = 2^{-10}$.

Figure 5.6 illustrates the numerical behavior predicted by the geometric interpretation of the convective contribution to enstrophy dynamics, as discussed in Remark 3.6.

In particular, we compare the enstrophy evolution of a classical $\mathbf{H}^1$–conforming scheme that is solely energy–stable against our proposed integrator (4.16), which enforces both energy and enstrophy stability. Initially, both methods exhibit rapid growth in enstrophy, i.e. the vorticity field exhibits tightly curved vortex lines, resulting in a pronounced convective contribution to the evolution of enstrophy. As dissipation takes effect, these curved structures gradually relax and straighten, reducing curvature–driven instabilities. Consequently, the convective term weakens, and the evolution of enstrophy stabilises. This aligns with the interpretation that curved vortex lines are energetically less stable: the flow becomes increasingly regular, and the enstrophy correspondingly more stable. While the term $\boldsymbol{\omega} \cdot \nabla \boldsymbol{\omega}$ does not measure curvature in the strict sense, its decomposition reveals that alignment with vortex–line curvature directly affects enstrophy production. The experiment does not seek new regularity results but probes whether the proposed energy–enstrophy discretisation moderates enstrophy growth versus a classical energy–only $\mathbf{H}^1$ scheme; it does, avoiding the large, resolution–dependent amplification seen for the energy–only method (cf. §1.1.3).

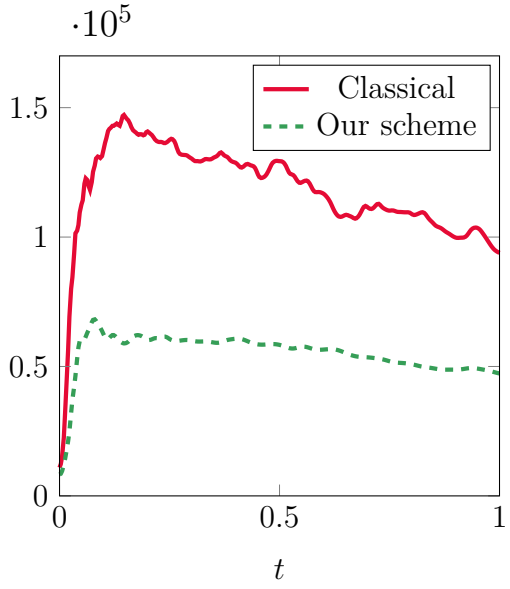

Figure 5.6: Enstrophy time series for both the classical $\mathbf{H}^1$–conforming scheme and our proposed conforming integrator (4.16). The initial rapid growth reflects tightly curved vortex lines and strong convective enstrophy production; dissipation then relaxes these structures and the enstrophy stabilises.

« Le vent se lève ! . . . il faut tenter de vivre ! »

"The wind is rising ! . . . we must try to live !"

— Paul Valéry, *Le Cimetière marin* (1920)

6

Discussion and Outlook

This work presents the application of auxiliary variables to enforce conservation laws and dissipation inequalities, as proposed by Andrews & Farrell [AF25], yielding a mixed velocity–vorticity finite–element integrator for the incompressible Navier–Stokes equations that preserves, at the discrete level, the continuous balance laws for kinetic energy $\mathcal{K}(\mathbf{u}) = \frac{1}{2}\|\mathbf{u}\|^2$ and enstrophy $\mathcal{E}(\mathbf{u}) = \frac{1}{2}\|\nabla\mathbf{u}\|^2$ under any Gauss–Legendre time integration.

In 2D, the enstrophy balance implies an Re–independent $\mathbf{H}^1$–bound on the velocity (cf. Lemma 3.8). Although the construction introduces an auxiliary vorticity $\boldsymbol{\omega}$, the conservation/dissipation statements are enforced directly on the primal field $\mathbf{u}$, in contrast to MEEVC, where the exact invariant is tied to the auxiliary variable. This distinction is reflected in the shear layer test (see §5.1), where our integrator conserves both energy and enstrophy levels throughout the simulation, avoiding the oscillations and artificial dissipation observed in the classical and MEEVC runs, thereby exhibiting greater numerical stability on under–resolved meshes at high Reynolds numbers Re.

In 3D, conforming finite–element spaces required for the discretisation—such as $\mathbf{H}(\operatorname{grad}\operatorname{curl})$—are not generally available in mainstream FE software. To address this, a conforming variant of the scheme was derived in §4.3, enabling structure–preserving implementations in both two and three dimensions. As far as we are aware of, this constitutes the only conforming enstrophy–stable discretisation

implementable on any widely available FEEC software. The integrator was validated on the Hill vortex problem (see §5.3), designed to examine the behaviour of enstrophy preservation in the three dimensional setting. In two dimensions, the vortex test reproduced the expected inviscid dynamics with consistent conservation of energy and enstrophy. To conclude, and as promised in §1.1.2, the deficiencies illustrated in Figure 1.1 are now resolved: the vortex maintains its structure, the invariants are preserved, and the dynamics unfold without artificial dissipation or oscillation.

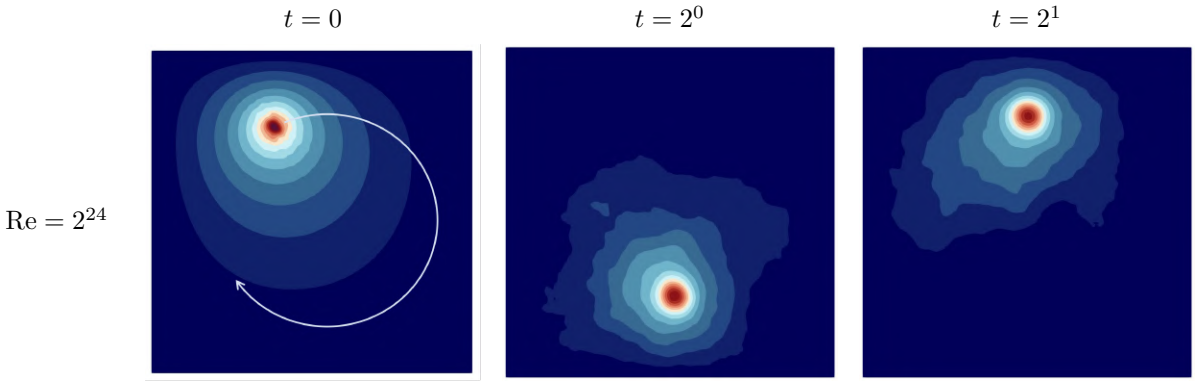

Figure 6.1: Snapshots of an energy– and enstrophy–stable scheme for $\mathrm{Re} = 2^{24}$ at times $t \in \{0, 2^0, 2^1\}$ (cf. Figure 1.1).

In view of these results, several directions appear both natural and feasible. On the modelling side, extending the discretisation to domains with non–trivial topology (i.e. an annulus) will require working "modulo cohomology," i.e. enforcing global flux/circulation constraints to eliminate discrete harmonic fields, while retaining the balance laws. Beyond flat domains, the idea naturally extends to Riemannian manifolds and bundle–valued fields: the balances become metric identities for differential forms, and the convective terms can be written as Lie derivatives/Poisson brackets. This opens a route to structure–preserving integrators on curved surfaces and embedded manifolds, provided metric terms and connections are discretised with commuting projections. Lastly, in 3D, helicity is a fundamental invariant of ideal flow. One may try to enforce discrete conservation of helicity along with energy and enstrophy, thereby probing how preserving vortex–line topology interacts with enstrophy production in three dimensions.

Appendices

「道可道，非常道；名可名，非常名。」

"The Way that can be spoken is not the enduring Way; the name that can be named is not the enduring name."

— Laozi, *Tao Te Ching*, Chapter 1

A

2D vortex test

Appendix A presents supplementary visualisations supporting the numerical experiments discussed in §5.2. Figure A.1 illustrate the qualitative behaviour of the flow fields under different discretisation schemes and parameter regimes.

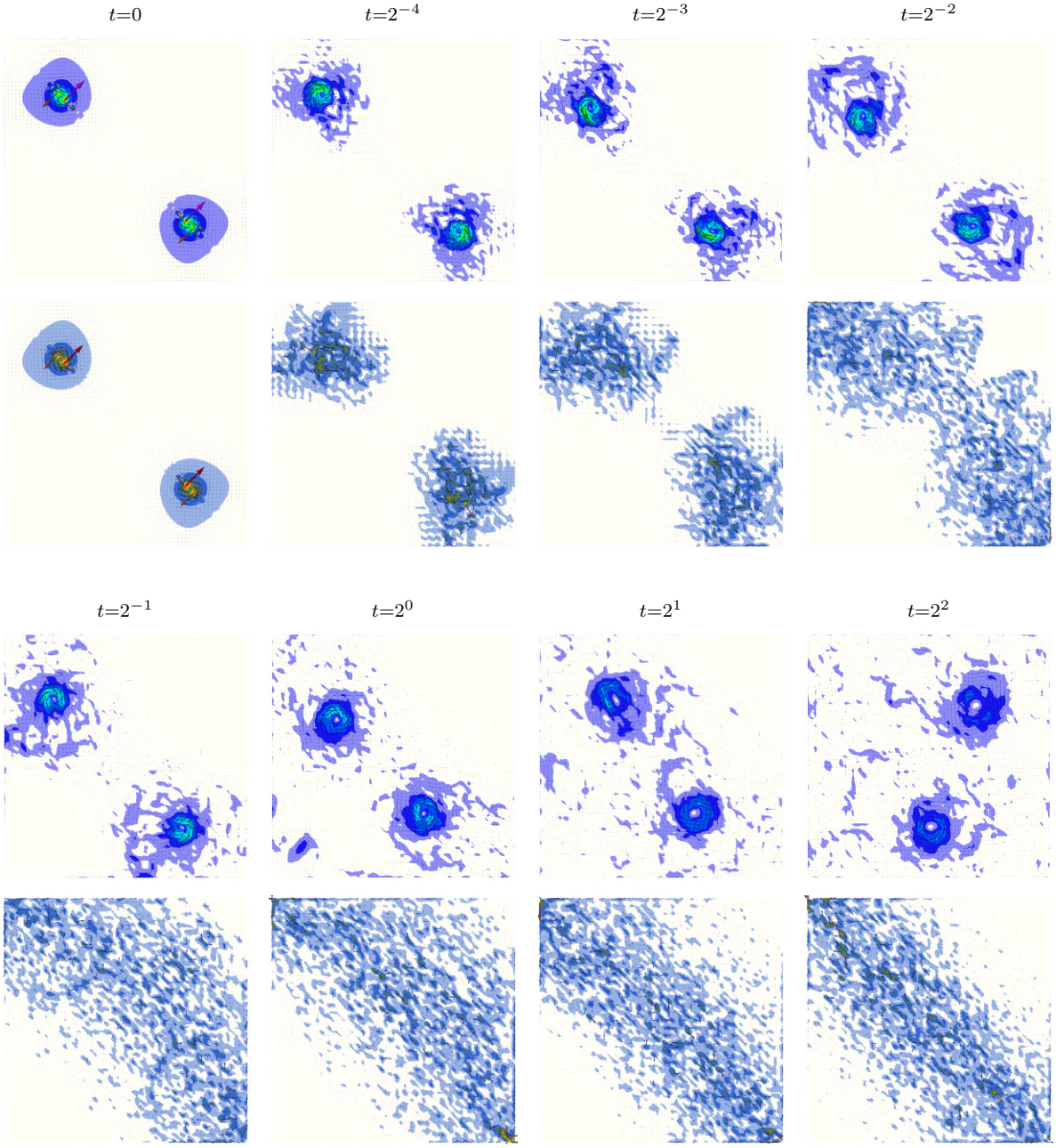

Figure A.1: 2D vortex evolution at 8 time steps $t = \{0, 2^{-4}, 2^{-3}, 2^{-2}, 2^{-1}, 2^{0}, 2^{1}, 2^{2}\}$. Top block: proposed (top row) vs. classical (bottom row) for the first 4 time steps; bottom block: same comparison for the final 4 steps. Square aspect ratio preserved. Colormaps with matched visual characteristics were chosen to facilitate comparison between the two schemes across time.

'Tis but a ring where we come and we go;
Beginning there is none, nor end, we know;
And none there is to tell us plainly this—
Whence have we come, and whither shall we go?

—Khayyām, *Rubāīyāt* (tr. E. H. Whinfield, 1883)

References

[AGL05] J. Ahrens, B. Geveci, & C. Law. "ParaView: An End–User Tool for Large Data Visualization". In: *Visualization Handbook*. Ed. by C. D. Hansen & C. R. Johnson. Elsevier, 2005. DOI: 10.1016/B978-012387582-2/50038-1.

[AP24a] M. Ainsworth & C. Parker. "Computing H^2–conforming finite element aproximations without having to implement C^1–elements". In: *SIAM Journal on Scientific Computing* 46.4 (2024), A2398–A2420. DOI: 10.1137/23M1615486.

[AP24b] M. Ainsworth & C. Parker. "Two and three dimensional H^2–conforming finite element approximations without C^1–elements". In: *Computer Methods in Applied Mechanics and Engineering* 431 (2024), p. 117267. DOI: 10.1016/j.cma.2024.117267.

[Alf84] P. Alfeld. "A trivariate Clough–Tocher scheme for tetrahedral data". In: *Computer Aided Geometric Design* 1.2 (1984), pp. 169–181. DOI: 10.1016/0167-8396(84)90029-3.

[Aln+14] M. S. Alnæs et al. "Unified form language: A domain–specific language for weak formulations of partial differential equations". In: *ACM Transactions on Mathematical Software* 40.2 (2014). DOI: 10.1145/2566630.

[Aln+15] M. S. Alnaes et al. "The FEniCS Project Version 1.5". In: *Archive of Numerical Software* 3 (2015). DOI: 10.11588/ans.2015.100.20553.

[AF25] B. D. Andrews & P. E. Farrell. *Enforcing conservation laws and dissipation inequalities numerically via auxiliary variables*. 2025. DOI: 10.48550/arXiv.2407.11904.

[Ara66] A. Arakawa. "Computational design for long–term numerical integration of the equations of fluid motion: Two–dimensional incompressible flow. Part I". In: *Journal of Computational Physics* 1.1 (1966), pp. 119–143. DOI: 10.1016/0021-9991(66)90015-5.

[AL77] A. Arakawa & V. R. Lamb. "Computational design of the basic dynamical processes of the UCLA general circulation model". In: *General Circulation Models of the Atmosphere*. Ed. by J. Chang. Vol. 17. Methods in Computational Physics: Advances in Research and Applications. Elsevier, 1977, pp. 173–265. DOI: 10.1016/B978-0-12-460817-7.50009-4.

[Arn18] D. N. Arnold. *Finite Element Exterior Calculus*. CBMS-NSF Regional Conference Series in Applied Mathematics. Society for Industrial & Applied Mathematics, 2018. DOI: 10.1137/1.9781611975543.

[AFW06] D. N. Arnold, R. S. Falk, & R. Winther. "Finite Element Exterior Calculus, Homological Techniques, and Applications". In: *Acta Numerica* 15 (2006), pp. 1–155. DOI: 10.1017/S0962492906210018.

[AFW09] D. N. Arnold, R. S. Falk, & R. Winther. "Finite Element Exterior Calculus: From Hodge Theory to Numerical Stability". In: *Bulletin of the American Mathematical Society* 47 (2009). DOI: 10.1090/S0273-0979-10-01278-4.

[AK08] V. I. Arnold & B. A. Khesin. *Topological Methods in Hydrodynamics*. Springer Science & Business Media, 2008. ISBN: 978-0-387-22589-0.

[BC17] S. Blanes & F. Casas. *A Concise Introduction to Geometric Numerical Integration*. CRC Press, 2017. DOI: 10.1201/b21563.

[BH06] P. B. Bochev & J. M. Hyman. "Principles of mimetic discretizations of differential operators". In: *Compatible Spatial Discretizations*. Ed. by D. N. Arnold et al. Springer New York, 2006, pp. 89–119. DOI: 10.1007/0-387-38034-5_5.

[Bos98] A. Bossavit. "On the geometry of electromagnetism". In: *J. Japan Soc. Appl. Electromagn. Mech.* 6.1-4 (1998), pp. 17–28, 114–23, 114–23, 233–40, 318–26. URL: https://faculty.washington.edu/seattle/physics544/2011-lectures/bossavit.pdf.

[BDM85] F. Brezzi, J. Douglas, & L. D. Marini. "Two families of mixed finite elements for second order elliptic problems". In: *Numerische Mathematik* 47 (1985), pp. 217–235. DOI: 10.1007/BF01389710.

[BK25] P. D. Brubeck & R. C. Kirby. *FIAT: enabling classical and modern macroelements*. 2025. DOI: 10.48550/arXiv.2501.14599.

[BP03] C. J. Budd & M. D. Piggott. "Geometric integration and its applications". In: *Handbook of Numerical Analysis*. Vol. XI. Amsterdam: North–Holland Publishing Co., 2003, pp. 35–139. DOI: 10.1016/S1570-8659(02)11002-7.

[BF07] E. Burman & M. A. Fernández. “Continuous interior penalty finite element method for the time-dependent Navier–Stokes equations”. In: *Numerische Mathematik* 107.1 (2007), pp. 39–77. DOI: 10.1007/s00211-007-0070-5.

[BFH06] E. Burman, M. A. Fernández, & P. Hansbo. “Continuous interior penalty finite element method for Oseen’s equations”. In: *SIAM Journal on Numerical Analysis* 44.3 (2006), pp. 1248–1274. DOI: 10.1137/040617686.

[BH04] E. Burman & P. Hansbo. “Edge stabilization for Galerkin approximations of convection–diffusion–reaction problems”. In: *Computer Methods in Applied Mechanics and Engineering*. Recent Advances in Stabilized and Multiscale Finite Element Methods 193.15 (2004), pp. 1437–1453. DOI: 10.1016/j.cma.2003.12.032.

[CH24] L. Chen & X. Huang. “Finite element de Rham and Stokes complexes in three dimensions”. In: *Mathematics of Computation* 93.345 (2024), pp. 55–110. DOI: 10.1090/mcom/3859.

[CMO11] S. H. Christiansen, H. Z. Munthe-Kaas, & B. Owren. “Topics in structure–preserving discretization”. In: *Acta Numerica* 20 (2011), pp. 1–119. DOI: 10.1017/S096249291100002X.

[CT65] R. W. Clough & J. L. Tocher. “Finite element stiffness matrices for analysis of plate bending”. In: *Proceedings of the First Conference on Matrix Methods in Structural Mechanics* (1965), pp. 515–546.

[CKS00] B. Cockburn, G. E. Karniadakis, & C.-W. Shu. “The development of discontinuous Galerkin methods”. In: *Discontinuous Galerkin Methods*. Berlin: Springer, 2000, pp. 3–50. DOI: 10.1007/978-3-642-59721-3_1.

[CD00] M. Costabel & M. Dauge. “Singularities of electromagnetic fields in polyhedral domains”. In: *Archive for Rational Mechanics and Analysis* 151.3 (2000), pp. 221–276. DOI: 10.1007/s002050050197.

[Cot23] C. J. Cotter. “Compatible finite element methods for geophysical fluid dynamics”. In: *Acta Numerica* 32 (2023), pp. 291–393. DOI: 10.1017/S0962492923000028.

[DD76] J. Douglas Jr. & T. Dupont. “Interior penalty procedures for elliptic and parabolic Galerkin methods”. In: *Computing Methods in Applied Sciences*. Vol. 58. Lecture Notes in Physics. Berlin: Springer Verlag, 1976, pp. 207–216. DOI: 10.1007/BFb0120591.

[EG21a] A. Ern & J.-L. Guermond. *Finite Elements I: Approximation and Interpolation*. Vol. 72. Texts in Applied Mathematics. Cham, Switzerland: Springer International Publishing, 2021. DOI: 10.1007/978-3-030-56341-7.

[EG21b] A. Ern & J.-L. Guermond. *Finite Elements II: Galerkin Approximation, Elliptic and Mixed PDEs*. Vol. 73. Texts in Applied Mathematics. Cham, Switzerland: Springer International Publishing, 2021. DOI: 10.1007/978-3-030-56923-5.

[FKM21] P. E. Farrell, R. C. Kirby, & J. Marchena-Menéndez. "Irksome: Automating Runge–Kutta time-stepping for finite element methods". In: *ACM Transactions on Mathematical Software* 47.4 (2021), 30:1–30:26. DOI: 10.1145/3466168.

[FMS24] P. E. Farrell, L. Mitchell, & L. R. Scott. "Two conjectures on the Stokes complex in three dimensions on Freudenthal meshes". In: *SIAM Journal on Scientific Computing* 46.2 (2024), A629–A644. DOI: 10.1137/22M1533943.

[Fef00] C. L. Fefferman. *Existence and Smoothness of the Navier–Stokes Equation*. Tech. rep. Millennium Prize Problem statement. Clay Mathematics Institute, 2000.

[Fra11] T. Frankel. *The Geometry of Physics: An Introduction*. 3rd ed. Cambridge University Press, 2011. DOI: 10.1017/CBO9781139061377.

[FGN20] G. Fu, J. Guzmán, & M. Neilan. "Exact smooth piecewise polynomial sequences on Alfeld splits". In: *Mathematics of Computation* 89.323 (2020), pp. 1059–1091. DOI: 10.1090/mcom/3520.

[Gaf55] M. P. Gaffney. "Hilbert space methods in the theory of harmonic integrals". In: *Transactions of the American Mathematical Society* 78 (1955), pp. 426–444. DOI: 10.1090/S0002-9947-1955-0068888-1.

[Ger12] M. Gerritsma. "An introduction to a compatible spectral discretization method". In: *Mechanics of Advanced Materials and Structures* 19 (2012), pp. 48–67. DOI: 10.1080/15376494.2011.572237.

[GR12] V. Girault & P.-A. Raviart. *Finite Element Methods for Navier-Stokes Equations: Theory and Algorithms*. Springer Science & Business Media, 2012. DOI: 10.1007/978-3-642-61623-5.

[GN18] J. Guzmán & M. Neilan. "Inf–sup stable finite elements on barycentric refinements producing divergence–free approximations in arbitrary dimensions". In: *SIAM Journal on Numerical Analysis* 56.5 (2018), pp. 2826–2844. DOI: 10.1137/17M1153467.

[HLW06] E. Hairer, C. Lubich, & G. Wanner. *Geometric Numerical Integration: Structure–Preserving Algorithms for Ordinary Differential Equations*. Heidelberg, Germany: Springer Science & Business Media, 2006. DOI: 10.1007/3-540-30666-8.

[Ham+23] D. A. Ham et al. *Firedrake User Manual*. First edition. Imperial College London et al. 2023. DOI: 10.25561/104839.

[Han23] M.-L. Hanot. "An arbitrary order and pointwise divergence–free finite element scheme for the incompressible 3D Navier–Stokes equations". In: *SIAM Journal on Numerical Analysis* 61.2 (2023), pp. 784–811. DOI: 10.1137/21M1443686.

[HW65] F. J. Harlow & J. E. Welch. "Numerical calculation of time–dependent viscous incompressible flow of fluid with free surface". In: *Physics of Fluids* 8.12 (1965), p. 2182. DOI: 10.1063/1.1761178.

[Hec12] F. Hecht. "New development in freefem++". In: *Journal of Numerical Mathematics* 20.3-4 (2012), pp. 251–266. ISSN: 1569-3953. DOI: 10.1515/jnum-2012-0013.

[Hil94] M. J. M. Hill. "VI. On a spherical vortex". In: *Philosophical Transactions of the Royal Society of London. (A.)* 185 (1894), pp. 213–245. DOI: 10.1098/rsta.1894.0006.

[Hip01] R. Hiptmair. "Higher order Whitney forms". In: *Progress in Electromagnetics Research* 32 (2001), pp. 271–299. DOI: 10.1163/156939301X00490.

[Hu25] K. Hu. *Many facets of cohomology: Differential complexes and structure–aware formulations*. 2025. DOI: 10.48550/arXiv.2503.22813.

[HZZ22] K. Hu, Q. Zhang, & Z. Zhang. "A family of finite element Stokes complexes in three dimensions". In: *SIAM Journal on Numerical Analysis* 60.1 (2022), pp. 222–243. DOI: 10.1137/20M1358700.

[IQ18] A. Iserles & G. R. W. Quispel. "Why Geometric Numerical Integration?" In: *Discrete Mechanics, Geometric Integration and Lie–Butcher Series*. Ed. by K. Ebrahimi-Fard & M. Barbero Liñán. Springer Proceedings in Mathematics & Statistics. Cham: Springer International Publishing, 2018, pp. 1–28. DOI: 10.1007/978-3-030-01397-4_1.

[KYP20] D. Kang, D. Yun, & B. Protas. "Maximum amplification of enstrophy in three–dimensional Navier–Stokes flows". In: *Journal of Fluid Mechanics* 893 (2020), A22. DOI: 10.1017/jfm.2020.204.

[KPG11] J. Kreeft, A. Palha, & M. Gerritsma. *Mimetic Framework on Curvilinear Quadrilaterals of Arbitrary Order*. 2011. DOI: 10.48550/arXiv.1111.4304.

[LE01] J.-G. Liu & W. E. "Simple finite element method in vorticity formulation for incompressible flows". In: *Mathematics of Computation* 70.234 (2001), pp. 579–593. DOI: 10.1090/S0025-5718-00-01239-4.

[LS00] J.-G. Liu & C.-W. Shu. "A high–order discontinuous Galerkin method for 2D incompressible flows". In: *Journal of Computational Physics* 160.2 (May 2000), pp. 577–596.

[MT89] Y. Maday & E. Tadmor. "Analysis of the spectral vanishing viscosity method for periodic conservation laws". In: *SIAM Journal on Numerical Analysis* 26.4 (1989), pp. 854–870. DOI: 10.1137/0726047.

[MA76] F. Mesinger & A. Arakawa. *Numerical methods used in atmospheric models*. Report. Global Atmospheric Research Programme, 1976.

[Mof69] H. K. Moffatt. "The degree of knottedness of tangled vortex lines". In: *Journal of Fluid Mechanics* 35.1 (Jan. 1969), pp. 117–129. ISSN: 1469-7645, 0022-1120. DOI: 10.1017/S0022112069000991.

[MS75] J. Morgan & R. Scott. "A nodal basis for C^1 piecewise polynomials of degree $n \geq 5$". In: *Mathematics of Computation* 29.131 (1975), pp. 736–740. DOI: 10.1090/S0025-5718-1975-0375740-7.

[MSP15] R. C. Moura, S. J. Sherwin, & J. Peiró. "Linear dispersion–diffusion analysis and its application to under–resolved turbulence simulations using discontinuous Galerkin spectral/*hp* methods". In: *Journal of Computational Physics* 298 (2015), pp. 695–710. DOI: 10.1016/j.jcp.2015.06.020.

[Mou+17] R. C. Moura et al. "On the eddy–resolving capability of high–order discontinuous Galerkin approaches to implicit LES / under–resolved DNS of Euler turbulence". In: *Journal of Computational Physics* 330 (2017), pp. 615–623. DOI: 10.1016/j.jcp.2016.10.056.

[Mou+22] R. C. Moura et al. "Gradient jump penalty stabilisation of spectral/*hp* element discretisation for under–resolved turbulence simulations". In: *Computer Methods in Applied Mechanics and Engineering* 388 (2022). DOI: 10.1016/j.cma.2021.114200.

[Néd86] J.-.-C. Nédélec. "A new family of mixed finite elements in $\mathbb{R}^3$". In: *Numerische Mathematik* 50.1 (1986), pp. 57–81. DOI: 10.1007/BF01389668.

[Nei15] M. Neilan. "Discrete and conforming smooth de Rham complexes in three dimensions". In: *Mathematics of Computation* 84.295 (2015), pp. 2059–2081. DOI: 10.1090/S0025-5718-2015-02958-5.

[Oxf25] U. of Oxford. *Use of generative AI tools to support learning*. https://www.ox.ac.uk/students/academic/guidance/skills/ai-study. accessed 10 September 2025. 2025.

[PG17] A. Palha & M. Gerritsma. "A mass, energy, enstrophy and vorticity conserving (MEEVC) mimetic spectral element discretization for the 2D incompressible Navier–Stokes equations". In: *Journal of Computational Physics* 328 (2017), pp. 200–220. DOI: 10.1016/j.jcp.2016.10.009.

[Phi59] N. A. Phillips. "An example of non–linear computational instability". In: *The Atmosphere and the Sea in Motion* 501 (1959), p. 504.

[PW70] S. A. Piacsek & G. P. Williams. "Conservation properties of convection difference schemes". In: *Journal of Computational Physics* 6.3 (1970), pp. 392–405. DOI: 10.1016/0021-9991(70)90038-0.

[RP20] Y. Renard & K. Poulios. "GetFEM: Automated FE modeling of multiphysics problems based on a generic weak form language". In: *ACM Trans. Math. Softw.* 47.1 (2020), 4:1–4:31. DOI: 10.1145/3412849.

[Rob20] J. C. Robinson. "The Navier–Stokes regularity problem". In: *Philosophical Transactions of the Royal Society A: Mathematical, Physical and Engineering Sciences* 378.2174, 20190526 (2020). DOI: 10.1098/rsta.2019.0526.

[SV85a] L. R. Scott & M. Vogelius. "Conforming finite element methods for incompressible and nearly incompressible continua". In: *Large Scale Computations in Fluid Mechanics*. Vol. 22. Providence: American Mathematical Society, 1985, pp. 221–244.

[SV85b] L. R. Scott & M. Vogelius. "Norm estimates for a maximal right inverse of the divergence operator in spaces of piecewise polynomials". In: *ESAIM: Mathematical Modelling and Numerical Analysis* 19.1 (1985), pp. 111–143. DOI: 10.1051/m2an/1985190101111.

[Sha25] M. Shams. *MMSC*. https://github.com/matin-shams/MMSC. Accessed: 2025-09-07. 2025.

[Ske95] R. D. Skeel. "Numerical Hamiltonian Problems (J. M. Sanz-Serna and M. P. Calvo)". In: *SIAM Review* 37.2 (1995), pp. 277–279. DOI: 10.1137/1037075.

[Tad90] E. Tadmor. "Shock capturing by the spectral viscosity method". In: *Computer Methods in Applied Mechanics and Engineering* 80.1 (1990), pp. 197–208. DOI: 10.1016/0045-7825(90)90023-F.

[Tad93] E. Tadmor. "Total variation and error estimates for spectral viscosity approximations". In: *Mathematics of Computation* 60.201 (1993), pp. 245–256. DOI: 10.1090/S0025-5718-1993-1153170-9.

[TC78] R. Temam & A. Chorin. "Navier Stokes Equations: Theory and Numerical Analysis". In: *Journal of Applied Mechanics* 45.2 (1978), pp. 456–456. DOI: 10.1115/1.3424338.

[Ton71] E. Tonti. "On the Mathematical Structure of a Large Class of Physical Theories". In: *Rendiconti dell'Accademia Nazionale dei Lincei* 52 (1971), pp. 1–13.

[Ton88] E. Tonti. "Algebraic Topology and Computational Electromagnetism". In: *4th International Meeting on the Fundamentals of Electromagnetism*. 1988, pp. 284–294.

[Zha+24] Y. Zhang et al. "A MEEVC discretization for two–dimensional incompressible Navier-Stokes equations with general boundary conditions". In: *Journal of Computational Physics* 510 (2024), p. 113080. DOI: 10.1016/j.jcp.2024.113080.